



**CHALMERS**  
UNIVERSITY OF TECHNOLOGY

---

# **Software for Calibration in Gamma-Ray Spectrometric *In-situ* Measurements**

Master's thesis in Nuclear Engineering

YE YUAN JOSEFSSON



**Software for Calibration in Gamma-Ray  
Spectrometric *In-situ* Measurements**

YE YUAN JOSEFSSON

Department of Chemical and Biological Engineering  
CHALMERS UNIVERSITY OF TECHNOLOGY  
Gothenburg, Sweden 2014

*Master's Thesis*

Software for Calibration in Gamma-Ray Spectrometric *In-situ* Measurements  
YE YUAN JOSEFSSON

©YE YUAN JOSEFSSON, 2014

Department of Chemical and Biological Engineering  
Division of Nuclear Chemistry  
CHALMERS UNIVERSITY OF TECHNOLOGY  
SE-412 96 Gothenburg  
Sweden  
Telephone: +46 (0) 31 - 772 10000

## Abstract

A gamma-ray spectrometric measurement on site, or *in-situ* in Latin, can identify and quantify the radionuclides after a radioactive fall-out and provide results quickly. The efficiency of such a measurement, also called the calibration factor, is depending on many parameters on the site. These parameters may consist of uncertainties, and the quality of the measurement result is given by the combined uncertainty.

A software, including graphical user interfaces, was developed in MatLab R2014b to provide the calibration factor and its combined uncertainty for *in-situ* gamma-ray spectrometric measurements. The field-of-view of the detector was also provided by the software. Depending on how the radionuclides were deposited on and/or in the soil, four deposition models were considered in this work. In order to estimate the combined uncertainty, a numerical approach was used. The samples for each input quantities were taken according to the Latin Hypercube Sampling (LHS). Moreover, the samples could be assumed to have either uniform, triangular or normal distribution.

The software gave reliable results about the calibration factor and its combined uncertainty. Also, the detector's field-of-view that was calculated was reasonable. However validations need to be performed for some of the models.

KEYWORDS:  $\gamma$ -spectrometric *in-situ* measurement, combined uncertainty, Latin Hypercube Sampling

## **Acknowledgements**

I would like to thank my examiner Chistian Ekberg and my supervisors Henrik Ramebäck and Torbjörn Nylén for giving me the opportunity to have this interesting project. A special thank to my supervisors for rewarding discussions and also advice and help they had given me during the this work. I would also like to thank Patrik Fredriksson for helping me with the MatLab. Finally, I would like to thank my family and my friends for their support.

Ye Yuan Josefsson  
Gothenburg, January 2015

# Contents

<b>1</b>	<b>Introduction</b>	<b>1</b>
1.1	Background . . . . .	1
1.2	Purpose . . . . .	2
1.3	Scope . . . . .	2
<b>2</b>	<b>Theory</b>	<b>3</b>
2.1	Gamma-Ray Spectrometry . . . . .	3
2.1.1	Ground-Level Gamma-Ray Spectrometry . . . . .	3
2.1.2	Detector Characteristics . . . . .	4
2.1.3	Field-of-view of a Detector . . . . .	4
2.2	Radioactivity Deposition Models . . . . .	4
2.2.1	Photon Fluence Rate . . . . .	5
2.2.2	Multiple Slabs Model . . . . .	8
2.2.3	Surface Deposition Model . . . . .	8
2.2.4	Volume Deposition Model . . . . .	8
2.2.5	Exponential Model . . . . .	9
2.3	Statistics and Data Analysis . . . . .	10
2.3.1	Monte Carlo Method . . . . .	10
2.3.2	Latin Hypercube Sampling . . . . .	11
2.3.3	Uncertainty Analysis . . . . .	13
<b>3</b>	<b>Method</b>	<b>15</b>
3.1	Sensitivity Analysis . . . . .	15
3.1.1	Results and Discussions . . . . .	16
3.2	Accuracy Investigation . . . . .	18
3.2.1	Results and Discussions . . . . .	19
<b>4</b>	<b>Results and Discussions</b>	<b>22</b>
4.1	Calibration Factor . . . . .	22
4.1.1	The Effects from Vegetation . . . . .	24
4.2	The Field-of-View of the Detector . . . . .	26
4.3	Combined Uncertainties . . . . .	28
4.4	Graphical User Interface . . . . .	30

<b>5</b>	<b>Conclusions</b>	<b>31</b>
<b>6</b>	<b>Further Work</b>	<b>32</b>
	References	34
	Appendix A	35
	Appendix B	37
	Appendix C	40
	Appendix D	41
	Appendix E	42
	Appendix F	44



# 1 | Introduction

Radioactivity has always been present in the environment due to the presence of natural radionuclides. There are three types of these radionuclides: primordial, cosmogenic and anthropogenic [1]. Since World War II, the radioactivity in the environment has been increased due to the release of anthropogenic radionuclides mainly from nuclear weapons testing and nuclear accidents.

Because the radioactivity may affect human health, it is essential to characterise and determine the level of the activity after a nuclear contamination as soon as possible. There are many kinds of radioactivity measurement methods. However, gamma-ray spectrometry on site, or *in-situ*, is an important technique regarding to these purposes. An *in-situ* measurement can identify the radionuclides on site and provide the amount of it directly after a completed measurement. Traditionally, sodium iodine (NaI) scintillators had been used, but since the development of detectors with higher resolution, e.g. the High-Purity germanium (HPGe) detector, these are today the primary choice for gamma-ray spectrometry [2].

## 1.1 Background

*In-situ* gamma-ray spectrometry using HPGe detectors is a powerful method to measure deposition of radionuclides. The HPGe detector is a semiconductor detector, which work similarly to a reverse biased diode [1]. When a gamma photon enters the depleted layer in the detector crystal, electron-hole pairs are formed and thereby charged are created, which are collected and a signal can be measured for its amplitude. This amplitude is proportional to the energy of the incoming gamma photon [1].

However, in order to achieve reliable measurement result with respect to activity, the efficiency of an HPGe detector needs to be calibrated for different gamma energies. In order to calibrate an HPGe detector in a laboratory, a standard solution containing a mixture of known radionuclides is often used. For an *in-situ* measurement the calibration is more difficult to perform because a source with known activity is not always available. Moreover, the measurement result on site depends on many parameters which may contain uncertainty and the combined measurement uncertainty is a measure of the quality of the measurement result.

## 1.2 Purpose

In this project the total efficiency of an *in-situ* gamma-ray spectrometry measurement was calibrated for models with different radionuclide deposition models, i.e. how the radioactivity is distributed in and/or on the ground. This efficiency is, for a specific detector, a function of incoming photon energy and its angle of incidence. Moreover, since the measurement uncertainty is an important component of the measurement result, this is also calculated by the software.

## 1.3 Scope

A MatLab program was designed for efficiency calculations of an HPGe detector. For every input photon energy the program will provide the measurement efficiency, including its combined uncertainty and also the detector's field-of-view. A graphical user interface was constructed in MatLab in order to give a more user-friendly program.

Fluctuations of the ground surface influence the measurement results and are difficult to handle [3]. In this work the surface is assumed to be perfectly plane, the activity and the density distribution in any compartment in the soil are assumed to be homogeneously distributed, and any object above the ground is not included in the models.

## 2 | Theory

The following theories give basic knowledge about *in-situ* gamma-ray spectrometry and hence a deeper understanding of the development of different models. In later part of this chapter there is some information about statistics used in this project.

### 2.1 Gamma-Ray Spectrometry

Monoenergetic photons that traveling through a uniform material attenuate according to an exponential function [2]

$$I = I_0 e^{-\mu r} \quad (2.1)$$

where  $I$  is the number of photons transmitted without change of the original energy,  $I_0$  is the number of original photons,  $\mu$  is the linear attenuation coefficient with dimension  $\text{m}^{-1}$  and  $r$  is the length of the path  $\text{m}$ . The mass attenuation coefficient,  $\mu/\rho$ , is also convenient to use because its values can easily be found in databases from *e.g.* the National Institute of Standards and Technology (NIST) [4].

#### 2.1.1 Ground-Level Gamma-Ray Spectrometry

The total efficiency, also called the calibration factor (CF), of a detector for *in-situ* measurements can be expressed as [5]

$$\frac{\dot{N}}{A_x} = \frac{\dot{N}}{\dot{N}_0} \cdot \frac{\dot{N}_0}{\varphi} \cdot \frac{\varphi}{A_x} \quad (2.2)$$

where  $\dot{N}$  is the full-energy peak count rate in cps,  $\dot{N}_0$  the full-energy peak count rate  $\text{s}^{-1}$  for photon incidence that is normal to the detector surface,  $\varphi$  the fluence rate per unit soil concentration  $\text{m}^{-2}\text{s}^{-1}$  or  $\text{m}^{-3}\text{s}^{-1}$  and  $A_x$  the source activity, which can have different dimensions.

The first ratio on the right-hand side can be expressed as a correction factor due to the unparallel incidence of the photon, the second one the peak response and the last one the fluence. The photon fluence rate,  $\varphi$ , is depending on the chosen deposition model and will be discussed later in this section.

### 2.1.2 Detector Characteristics

The first two ratios in Equation 2.2 can be denoted as the detector efficiency and depends on the detector characteristics, e.g. detector diameter and length. This is often determined empirically for a particular detector. For the HPGe detector used in this project the detector efficiency as a function of energy and angle of incidence had been developed by curve-fitting of measurement results [6], see Equation 2.3.

$$\varepsilon_{det}(\theta, E) = \exp \left[ a_1 + a_2\theta + a_3\theta^2 + a_4E + \frac{a_5}{E} + a_6 \cos \left( \frac{a_7\theta}{E^{a_8}} - a_9 \right) + a_{10}\ln E + a_{11}(\ln E)^2 \right] \quad (2.3)$$

where  $a_1 \sim a_{11}$  are parameters without physical interpretations,  $\theta$  is the photon incident angle in rad and  $E$  the photon energy in keV. The values for the parameters of the detector used in this work that are obtained after curve-fitting can be found in Table A.1 in Appendix A.

### 2.1.3 Field-of-view of a Detector

Ideally, the field-of-view of a detector is infinite if the surface is perfectly plane. Since the photons that are emitted from remote regions may be attenuated before they reach the detector, the contribution from the remote region decreases. Within a distance,  $R_{max}$ , the contribution of number of counts are a certain percentage of the total number of counts from the whole area [3]. For example, if 95% of the detector counts origin within a radius of 10 m, the detector should then be places at least 10 m away from anything that might interfere the measurement. This will make measurement over a large area more reliable. The distance  $R_{max}$ , hereafter called the detector field-of-view, can easily be expressed with the photon incidence angle  $\theta_{max}$ ,

$$R_{max} = H \tan \theta_{max} \quad (2.4)$$

where  $H$  is the detector height over the ground in m.

## 2.2 Radioactivity Deposition Models

As stated in an earlier section, the photon flux will depend on how the radioactivity is distributed in and/or on the ground. The distribution of radionuclides in the soil will depend on many factors [3], e.g. the time after deposition, the properties of the soil, the weather and human activities on the site. In this project, four models were set up for description of possible source distributions.

- Surface deposition model, where the radioactivity is assumed to be homogeneously distributed on the ground surface

- Volume deposition model, where the radioactivity is assumed to be homogeneously distributed within a soil volume
- Multiple slabs model, where the radioactivity containing soil volume is divided in several layers, where each layer has a homogeneous activity distribution
- Exponential model, where the radioactivity is assumed to penetrate into the soil and decreases exponentially

### 2.2.1 Photon Fluence Rate

The fluence rate of the photon at energy  $E$  is given by [2]

$$\varphi = \frac{A_x \cdot p(E) \cdot C(E)}{4\pi R^2}, \quad (2.5)$$

where  $p(E)$  is the photon emission probability for energy  $E$  in %,  $C(E)$  is the attenuation factor for photon energy  $E$  and  $R$  is the distance between the source and the detector in m.

In order to describe the activity contribution more realistically, the whole radioactivity containing volume can be divided in several sub-volumes [7]. Each sub-volume, or slab, has individual thickness,  $d_i$ , uniformly distributed radioactivity and consists of a fraction of the total activity, see Figure 2.1.

According to Equation 2.5, the fluence rate from an infinitesimal volume is

$$d\varphi_v = \frac{A_v p(E) C(E)}{4\pi R^2} dV. \quad (2.6)$$

where  $A_v$  is the activity per unit volume and  $dV = r dr d\phi dz$  with  $\phi$  as the azimuthal angle. When integrating over the azimuthal angle a factor  $2\pi$  is introduced and the equation above becomes

$$d\varphi_v = \frac{A_v r}{2R^2} p(E) C(E) dr dz. \quad (2.7)$$

The photon fluence rate, which depends on the photon incidence angle, can be determined by setting  $r = H \tan\theta$  and  $dr = H(\cos\theta)^{-2} d\theta$ . Then the following equation is obtained:

$$d\varphi_v = \frac{A_v \tan\theta}{2} p(E) C(E) d\theta dz. \quad (2.8)$$

By rearranging Equation 2.1 the factor  $C(E)$  in Equation 2.8 is obtained

$$C(E) = \frac{I_0}{I} = \exp(-\mu r). \quad (2.9)$$

Because this factor is also depending on the material which the photon is passing through and the vertical distance between the detector and the source, hence in this report the

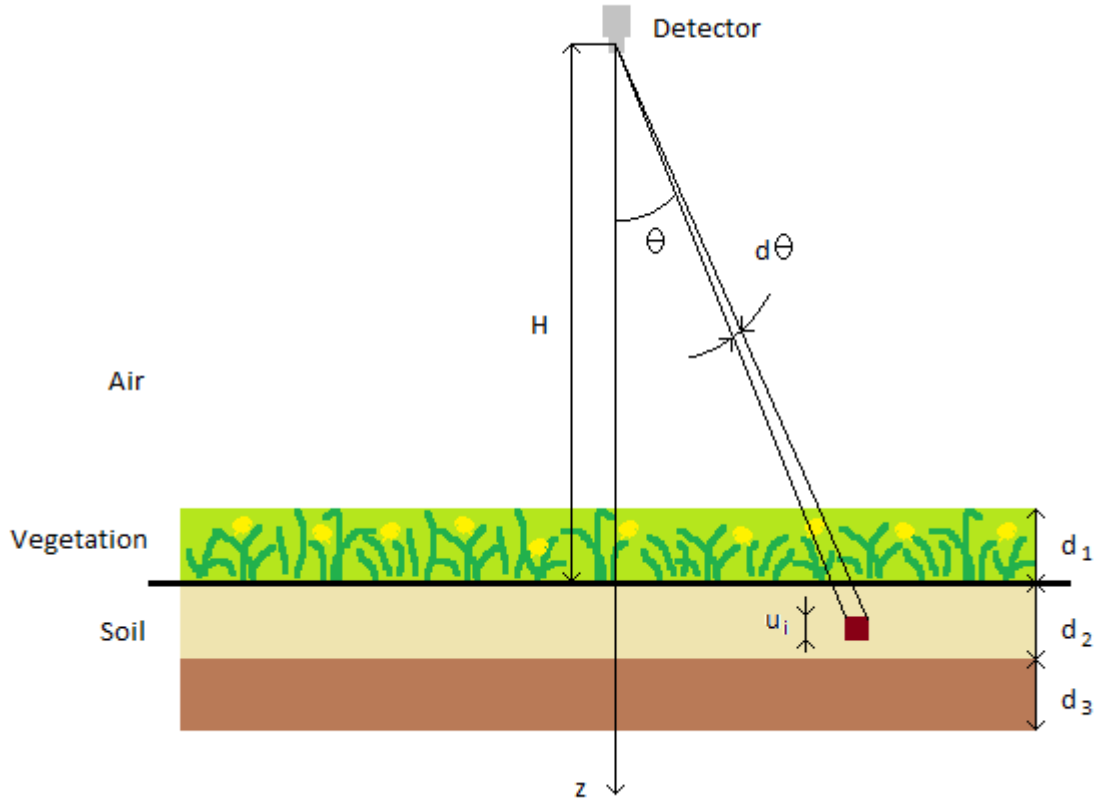


**Figure 2.1:** A schematic description of the arrangement of the slabs.

attenuation factor is written as

$$C_j(d) = \exp\left(-\frac{\mu_j d}{\cos\theta}\right) \quad (2.10)$$

where  $j$  is the current material and  $d$  is the vertical distance in m. If one considers the vegetation as one of the slabs, the total attenuation factor from slab  $i$  can be expressed as:

$$C_{tot,i} = C_{air}(H - d_1)C_{j,i}(u_i) \prod_{n=1}^{i-1} C_{j,n}(d_n) \quad (2.11)$$

where  $j$  can be either vegetation or soil.

## Photon Attenuation

A general description of the mass attenuation coefficient for soil,  $\mu_{soil}$  with unit  $m^{-1}$ , was developed earlier [8].

$$\frac{\mu_{soil}}{\rho_{soil}}(E) = 1.26 \cdot 10^5 E^{-4-27} + 0.142 E^{-0.445} - 2 \cdot 10^{-5}, \quad (2.12)$$

where the soil density  $\rho_{soil}$  is given in  $kg/m^3$  and the energy  $E$  in MeV. This description is valid for most types of soil and gives good results for photon energy within the range 0.3 to 3 MeV.

In order to approximate the attenuation coefficient for the vegetation, one can use a linear combination between the attenuation of air and the attenuation of water [3]. Consider a vegetation height of  $h_v$  in m and the mass per unit area of  $m_v$   $kg/m^2$ . Further assume that the density of the vegetation is  $\rho_{H_2O}$  when compressed. Then the attenuation coefficient can be expressed as

$$\mu_{veg} = \left(1 - \frac{m_v}{h_v \rho_{H_2O}}\right) \mu_{air} + \frac{m_v}{h_v \rho_{H_2O}} \mu_{H_2O}. \quad (2.13)$$

The observed values for linear attenuation coefficient for water and air,  $\mu_{H_2O}$  and  $\mu_{air}$  respectively, can be found in the NIST database [4]. The following equation was obtained after plotting values in log-log scale and then a curve-fitting was applied. For photon energy  $E$  in MeV the  $\mu_{H_2O}$  is

$$\mu_{H_2O}(E) = 100 \exp(-0.04(\ln E)^2 - 0.48 \ln E - 2.65) \quad (2.14)$$

The  $\mu_{air}$  is described as Equation 2.15, taken from Boson *et al.*[7].

$$\mu_{air}(E) = \rho_{air} 0.0623 E^{-0.4754} \quad (2.15)$$

These  $\mu$ s are given in  $m^{-1}$  and  $\rho_{air}$  in  $kg/m^3$ . The air density is assume to be a function depending on three parameters [9], the air pressure  $P$  given in kPa, the temperature  $T$  in  $^{\circ}C$  and the relative humidity  $h$  in %,

$$\rho_{air} = \frac{aP - (bT - c)h}{T + 273.16}, \quad \text{parameters} \quad \begin{cases} a = 3.348444 \\ b = 2.52 \cdot 10^{-5} \\ c = 2.0582 \cdot 10^{-4}. \end{cases} \quad (2.16)$$

To summarize, the photon fluence contribution from slab  $i$  with thickness  $d_i$  can then be expressed as

$$\varphi_i = \frac{A_v p(E)}{2} \iint C_{tot,i} \tan \theta du_i d\theta \quad (2.17)$$

with integration intervals

$$\begin{cases} 0 \leq u_i \leq d_i \\ 0 \leq \theta \leq \pi/2. \end{cases} \quad (2.18)$$

### 2.2.2 Multiple Slabs Model

The activity in each slab can be written in terms of total activity per unit area,  $A_s$ . The relation between the surface activity and the volume activity is

$$A_{v,i} = \frac{A_s k_i}{d_i}, \quad (2.19)$$

where  $d_i$  is the thickness of slab  $i$  and  $k_i$  is a proportional factor that describes the relative activity content in slab  $i$ . For total  $N$  slabs, the factor  $k_i$  can be expressed as

$$k_i = \frac{A_{v,i} d_i}{\sum_j^N A_{v,j} d_j}. \quad (2.20)$$

Then according to Equation 2.17 the calibration factor for the multiple slab model is

$$\frac{\dot{N}}{A_s} = \varepsilon_{det}(E, \theta) \frac{\varphi}{A_s} = \frac{p(E)}{2} \sum_i^N \frac{k_i}{d_i} \iint \varepsilon_{det}(E, \theta) C_{tot,i} \tan \theta du_i d\theta. \quad (2.21)$$

### 2.2.3 Surface Deposition Model

The radionuclides will initially after a deposition be deposited on the surface. In this model, assumption of uniformly distributed radionuclides on a perfectly flat surface is made. This is an ideal model because in reality, the radionuclides transported by the atmospheric process will not be distributed uniformly on the surface. To determine the calibration factor for a such model, take  $N = 1$  in equation 2.21 and assume simply that the soil slab is extremely thin. The vegetation above the ground surface can be assumed to be one of the slabs in multiple slab model. In such cases take  $N = 2$  in order to take the vegetation into account.

### 2.2.4 Volume Deposition Model

The radioactivity distribution may also be considered as uniform in the soil. Therefore the calibration factor for such a model can be obtained by taking  $N = 1$  in equation 2.21. If the vegetation above the ground surface is desired to be included, take instead  $N = 2$ .

However, soon after a radioactive fallout, radionuclides may penetrate a bit into the ground. In order to get a quick result of the calibration factor for a so-called emergency preparedness model [10], values in table 2.1 are assumed.



**Table 2.1:** Values used in calibration factor calculation for the emergency preparedness model. Ignore the last three values and set the relative activity content in the soil to 100% if there is no vegetation.

Parameter		Value
Soil layer thickness	[m]	0.02
Soil density	[kg/m <sup>3</sup> ]	500
Relative activity content	[%]	70
Vegetation height	[m]	0.1
Surface mass	[kg/m <sup>2</sup> ]	0.5
Relative activity content	[%]	30

### 2.2.5 Exponential Model

Another model that may be applied in *in-situ* gamma-ray spectrometry is when the concentration of radionuclides can be assumed to decrease exponentially with depth [5]:

$$A(z) = A_0 e^{-\alpha z}, \quad (2.22)$$

where  $A_0$  is the activity on the ground surface in unit Bq/m<sup>3</sup> and  $\alpha$  the reciprocal of the relaxation length of unit m<sup>-1</sup> for the radioactivity in the soil.

It is convenient to make a projection of the total activity in the soil on the surface by integration of equation 2.22 from 0 to  $\infty$  which gives  $A_a = A_0/\alpha$ . Insert equation 2.22 in equation 2.6 and set again  $r = (H + z) \tan \theta$ . The fluence rate is then obtained,

$$d\varphi = \frac{1}{2} p(E) \alpha A_a e^{-\alpha z} \tan \theta C(E) d\theta dz. \quad (2.23)$$

The attenuation factor above the ground is determined by an equivalent attenuation coefficient

$$\mu_{eq} = \left(1 - \frac{m_v}{H \rho_{H_2O}}\right) \mu_{air} + \frac{m_v}{H \rho_{H_2O}} \mu_{H_2O} \quad (2.24)$$

and the fluence rate can be rewritten as

$$d\varphi = \frac{p(E) \alpha A_a}{2} C_{eq}(H) \exp\left(-\frac{\alpha \cos \theta + \mu_{soil}}{\cos \theta} z\right) \tan \theta d\theta dz. \quad (2.25)$$

Integrating  $z$  from 0 to  $\infty$ , the previous equation becomes

$$d\varphi = \frac{p(E) \alpha A_a \sin \theta}{2(\alpha \cos \theta + \mu_{soil})} C_{eq}(H) d\theta \quad (2.26)$$

and finally the calibration factor for the exponential model is

$$\frac{\dot{N}}{A_a} = \int_0^{\pi/2} \frac{p(E) \sin \theta}{2(\cos \theta + \mu_{soil}/\alpha)} \varepsilon_{det}(E, \theta) C_{eq}(H) d\theta. \quad (2.27)$$

## 2.3 Statistics and Data Analysis

First of all, two important statistical quantities are defined. For total  $N$  samples, the sample mean and the sample variance are

$$\bar{x} = \frac{1}{N} \sum_{i=1}^N x_i \quad (2.28)$$

and

$$\sigma^2 = \frac{1}{N-1} \sum_{i=1}^N (x_i - \bar{x})^2. \quad (2.29)$$

In many measurements, the measurand is not measured directly, but is expressed as a function of other measurement quantities. In practice, a measurement result is only an estimate of the value of the measurand. Therefore, the uncertainty of that estimate must be included to give a complete measurement result [11]. Assume that the measurand  $Y$  can be written as a function of measurement quantities  $X_1, X_2, \dots, X_N$ ,

$$Y = f(X_1, X_2, \dots, X_N). \quad (2.30)$$

After  $N$  identical measurements, the estimate of  $Y$  can be taken as the mean of  $Y$

$$y = \bar{Y} = \frac{1}{n} \sum_{k=1}^n Y_k. \quad (2.31)$$

Further, assume that every input estimate of measurement quantity  $X_i$  consists of a standard uncertainty  $u(x_i)$ . This uncertainty can be of Type A, which is obtained by the statistical analysis of series of observations, and Type B, which is obtained by other methods than the statistical analysis of series of observations [11]. The combined uncertainty associated with  $Y$ ,  $u_c(y)$ , can be determined analytically as shown in Equation 2.32 [11]. This combined uncertainty will give a perception about the quality of the measurement result of  $Y$ .

$$u_c^2(y) = \sum_{i=1}^N \left( \frac{\partial f}{\partial x_i} \right)^2 u^2(x_i). \quad (2.32)$$

However, the function  $f$  is not always differentiable. In case of a complex relation between the input quantity and the measurand, a numerical approach may be convenient [12]. For input quantities  $X_1, X_2, \dots, X_N$  that are characterized by specific probability density functions (PDFs), the output will get a certain probability distribution. Then the combined uncertainty  $u_c(y)$  is simply the standard deviation of the outputs. A useful numerical method for the propagation of distributions is Monte Carlo methods [12].

### 2.3.1 Monte Carlo Method

Monte Carlo (MC) methods are a selection of methods that uses random samplings to solve problems [13, 12, 14]. Samples from predetermined PDFs are used in simulations

to obtain the probability distribution and other statistical properties of an unknown quantity. It is an old idea, scientists tried to determine the value of  $\pi$  using this idea centuries ago [13]. Nowadays, the MC methods are widely used within many scientific areas, e.g. physical science, engineering and finance. When using the MC method, one must deal with the precision and the accuracy of the simulation results.

The MC method works as follow.  $M$  values of quantities  $X_i, i = 1 \dots N$ , are selected randomly from their PDFs,  $p_{x_i}$ . Using these  $M$  values for each input quantity, an output set  $Y_k, k = 1, \dots, M$ , is obtained. This process can be seen as a repetition of the same experiment many times. Out of these  $Y_k$ s, the estimates of  $Y_k$  and its standard deviation  $s$  can be determined using Equation 2.33 respective 2.34.

$$\bar{Y}_k = \frac{1}{M} \sum_{k=1}^M Y_k = \frac{1}{M} \sum_{k=1}^M f(X_{1,k}, X_{2,k}, \dots, X_{N,k}) \quad (2.33)$$

$$s^2 = \frac{1}{M} \sum_{k=1}^M (Y_k - \bar{Y}_k)^2. \quad (2.34)$$

Due to this random sampling, the parameter values with low occurrence probability might be excluded from the input set if  $M$  is not large enough. Therefore, a large number of samples must be drawn to ensure that the input sets are representative for the parameter distributions and in turn avoid clusters in the output set. A large number of samples requires large computer memory and also means a long calculation time. However, these problems can be reduced by using a stratified sampling method [15], e.g. Latin Hypercube sampling.

### 2.3.2 Latin Hypercube Sampling

The Latin Hypercube Sampling (LHS) method is a special stratified sampling method that was developed by McKay *et al.* in 1979 [15]. Assume that the PDF for input quantity  $x_i$  is

$$p_{x_i}(\xi) = \int_0^\infty g_{x_i}(\xi) d\xi = 1. \quad (2.35)$$

The PDF for each input quantity is divided into  $M$  disjoint intervals, i.e. stratifications, so that

$$p_{x_i}(\xi) = \int_{I_k} g_{x_i}(\xi) d\xi, \quad k = 1, \dots, M, \quad (2.36)$$

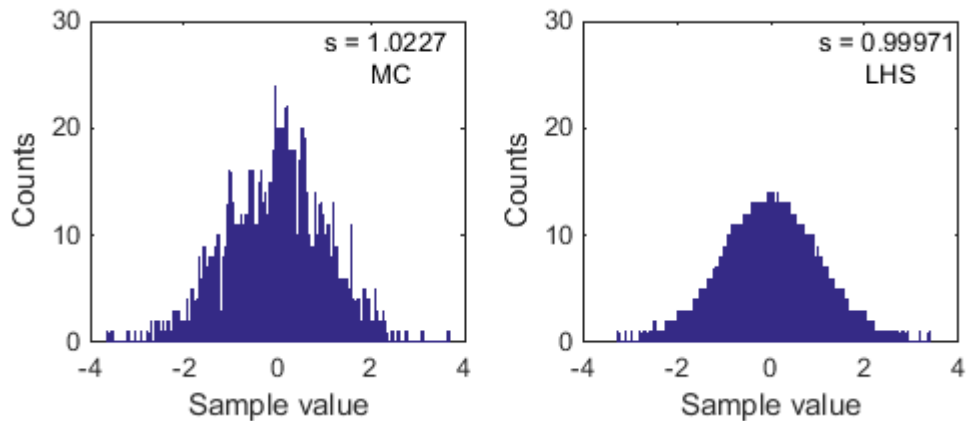
is equal for each interval  $I_k$ . Within every interval  $I_k$  one and only one sample is drawn randomly. By doing this,  $M$  samples are taken for each input quantity. The order of samples for each input quantity is shuffled randomly. Then the samples for each input quantity are randomly paired to form  $M$  input sets which in turn give an output set  $Y_k, k = 1, \dots, M$ . The outputs can then be analysed as in the case of using MC method.

The LHS method has several benefits compared to the MC methods. Using LHS, the

samples with low probability are forced to be represented in the input set. In this way, clusters in the output set are avoided even if a small number of calculations is performed. Earlier study has shown that it requires about 1/3 as many Latin Hypercube iterations as MC iterations to get equal results [16].

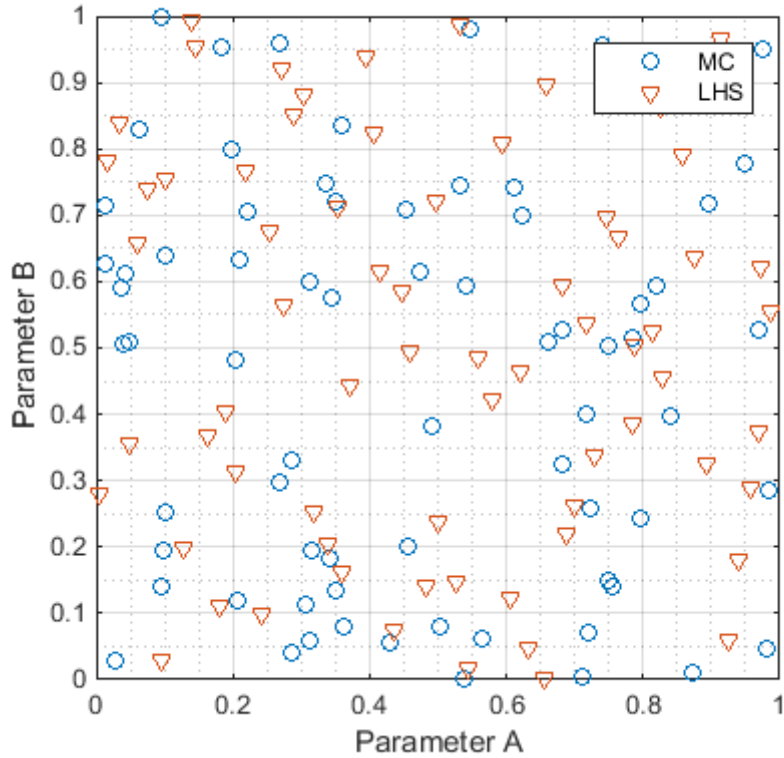
### Comparison between MC and LHS Methods

Figure 2.2 shows two sets of sample drawn using MC method respective LHS in histograms. The samples were drawn from the same normal distribution with  $\mu = 0$  and  $\sigma = 1$ . It can be seen that there is some clusters in the case of using the MC method. These clusters may cause clusters in the output set, which can affect the statistical properties of the outputs and that is not desirable.



**Figure 2.2:** 1 500 samples generated according to the MC method respective the LHS method, from the same normal distribution with  $\mu = 0$  and  $\sigma = 1$ . The standard deviation of the sample is also given.

Figure 2.3 shows two input sets containing samples that were generated according to the MC method respective the LHS method. Both parameter A and B were assumed to distribute according to the uniform distribution  $\mathcal{U}(0, 1)$ . As can be seen in Figure 2.3, the inputs generated according to the LHS method are more dispersed over the whole sample space and each stratification for the these two parameters had been represented once. In this way, clusters in the output set can be avoided.



**Figure 2.3:** Two input sets containing 70 samples generated according to the MC method respective the LHS method. Both parameter A and B were assumed to distribute uniformly between 0 and 1.

### 2.3.3 Uncertainty Analysis

The total uncertainty of the calibration factor consists of two components: the combined uncertainty of the detector efficiency calculation and the uncertainty from the calculations. According to Equation 2.32, the total uncertainty can be determined by

$$u_{total}^2 = u_{detector}^2 + u_{calculation}^2. \quad (2.37)$$

The combined uncertainty of the detector efficiency is a Type B uncertainty and was calculated to be 4% [6]. In order to determine the uncertainty from calculations, the following two concepts are useful.

### Law of Large Numbers [17]

The Law of Large Numbers (LLN) is a mathematical formulation which states that the sample mean of random variables  $X_i$  will converge towards the expectation value as the number of samples increases, i.e.

$$\mu = E[X_n] = \bar{X}_n = \lim_{n \rightarrow \infty} \frac{1}{n} \sum_{i=1}^n X_i \quad (2.38)$$

Consider that the PDF for every input quantity is stratified in  $N$  intervals, then  $N$  calibration factors (CF) will be obtained after calculations. According to the LLN, the estimate of the CF will converge towards the expectation value of the CF when  $N \rightarrow \infty$ . Also, the estimation of the uncertainty of the CF will converge towards the standard deviation of the CF. The relative uncertainty associated with calculations described in Equation 2.37 can be determined by the ratio between the standard deviation of the CF and the expectation value of the CF, i.e.

$$u_{\text{calculation}} = \bar{S}_N / \bar{Y}_N. \quad (2.39)$$

## 3 | Method

Initially, a simple sensitivity analysis was performed for the linear attenuation coefficient of air in order to reduce the amount of input quantities if possible. Models for the calibration factor calculation with different deposition types were implemented in MatLab (version R2014b) together with other necessary functions. The models were then modified to be able to be used for different purposes. Some user-friendly graphical user interfaces (GUIs) were build using a build-in interactive GUI construction kit, the GUI development environment (GUIDE).

To generate sample sets using the LHS method, build-in MatLab functions were used with some modifications. By assuming independence between all parameters, the covariances could be set to zero. The samples were generated as vectors, except for the soil condition parameters, e.g. the thickness and the density, where the samples were generated as matrices.

In order to be able to use LLN and CLT, the number of calculations must be large enough. So several tests were done in order to investigate how the relative uncertainty associated with calculations varies with the number of calculations. Also how the relation between the number of iterations and the number of calculations per iteration affects the uncertainties was investigated.

### 3.1 Sensitivity Analysis

Sensitivity analysis is performed in order to identify the most important ones among a large number of input parameters. In this project, how the linear attenuation coefficient of air,  $\mu_{air}$ , was affected by its input parameters was examined.  $\mu_{air}$  is a function of the photon energy and is proportional to the air density, see Equation 2.15. The air density is in turn depending on three parameters:

- the air pressure
- the air temperature
- the relative humidity in the air

There are many ways to perform a sensitivity analysis. In this project, the variation of  $\mu_{air}$  was investigated by fixing one of the three parameters of the air density and letting the other two vary. The variation range for the three parameters are shown in Table 3.1, and these ranges were chosen to adjust to the Swedish conditions [18, 19]. 10 000 samples were taken using LHS method for every parameter and they were paired randomly to form input sets to the calculation of  $\mu_{air}$ . Standard deviation were then taken for the  $\mu_{air}$ s, the parameter that resulted the smallest standard deviation was the most important one.

**Table 3.1:** Values used to examine the sensitivity of the linear attenuation coefficient of air [18, 19]. All parameters were assumed to be uniformly distributed.

		Average	Limits
Pressure	[kPa]	100	$\pm 10$
Temperature	[ $^{\circ}\text{C}$ ]	5	$\pm 20$
Relative humidity	[%]	80	$\pm 20$

### 3.1.1 Results and Discussions

The results of sensitivity analysis of  $\mu_{air}$  are shown in Figure 3.1, 3.2 and 3.3. Similar figures for two other photon energies can be found in Appendix B. The standard deviations for respective results are also shown in the figures. It is shown that the  $\mu_{air}$ s for fixed air pressure were least dispersed, which means that the air pressure is the most important parameter for the  $\mu_{air}$  calculation.

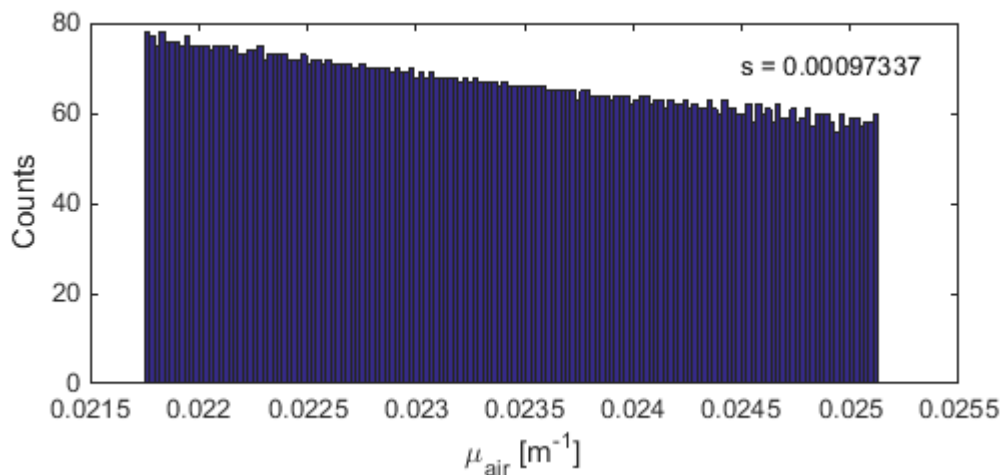


**Figure 3.1:**  $\mu_{air}$  for photon energy  $E = 100$  keV calculated when the pressure was fixed. The standard deviation of the results is shown in the corner.



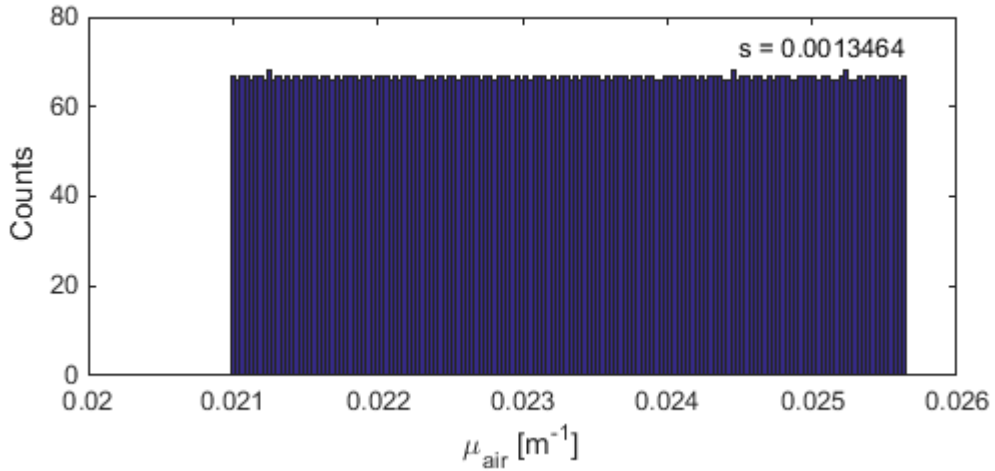


**Figure 3.2:**  $\mu_{air}$  for photon energy  $E = 100$  keV calculated when the temperature was fixed. The standard deviation of the results is shown in the corner.

The standard deviation of  $\mu_{air}$  is largest when the relative humidity was fixed. This means that the relative humidity is the least important parameter. Note that the relative humidity describes the relation between the amount of moisture (or water) and the maximal amount in the air at a certain temperature [19], the higher the relative humidity is, the more moist the air is. It is known that water has good attenuation ability, therefore the relative humidity should have significant impact on  $\mu_{air}$ . However, this relation can not be seen in the results from this sensitivity analysis. One might use an other description for  $\mu_{air}$  where the relative humidity has more significance. A linear combination of  $\mu_{air,dry}$  and  $\mu_{water}$  might be used, compare this idea with equation 2.15.

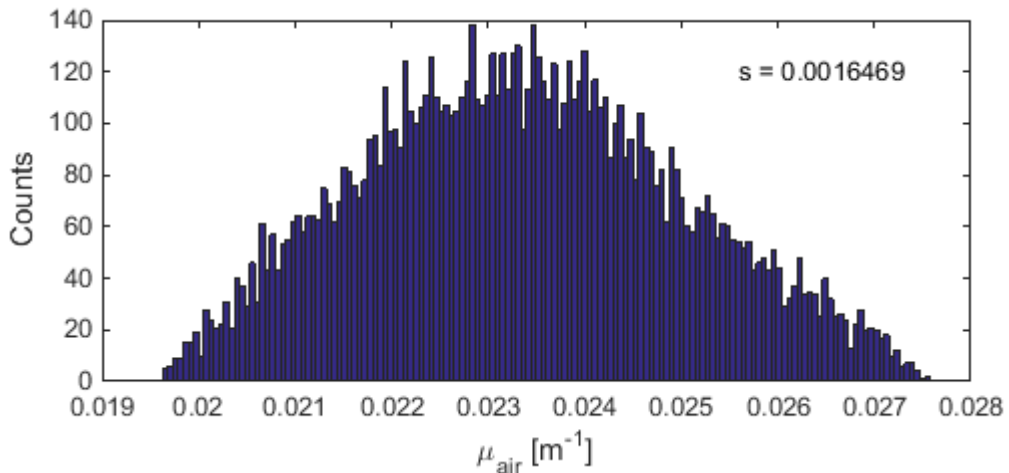


**Figure 3.3:**  $\mu_{air}$  for photon energy  $E = 100$  keV calculated when the relative humidity was fixed.

However, when determining  $\mu_{air}$  using equation 2.15, it results in that the relative humidity is not a significant parameter. This means that it has a small contribution to the uncertainty for calculation of the  $\mu_{air}$ , in turn the calculation of the calibration factor. Therefore the relative humidity will be designed to be an un-sampled parameter in the calibration calculation program.

Parameters that contribute to the combined uncertainty are shown in table 3.2. By assuming independence between all parameters, their individual contributions to the uncertainty can be determined. Set uncertainties of other parameters to zero, the deviation of the results will then only come from the parameter in question.

**Table 3.2:** table showing whether the parameter is contributing or not to the uncertainty of the calibration factor for different models. The  $\checkmark$  indicates "Yes" and  $\times$  "No".

Parameters	Models			
	Surface	Volume	Multiple slabs	Exponential
Detector height	$\checkmark$	$\checkmark$	$\checkmark$	$\checkmark$
Air pressure	$\checkmark$	$\checkmark$	$\checkmark$	$\checkmark$
Air temperature	$\checkmark$	$\checkmark$	$\checkmark$	$\checkmark$
Vegetation height	$\checkmark$	$\checkmark$	$\checkmark$	$\checkmark$
Surface mass	$\checkmark$	$\checkmark$	$\checkmark$	$\checkmark$
Activity content in veg.	$\checkmark$	$\checkmark$	$\checkmark$	$\times$
Soil slab thickness	$\times$	$\checkmark$	$\checkmark$	$\times$
Soil density	$\times$	$\checkmark$	$\checkmark$	$\checkmark$
Activity content in soil	$\checkmark$	$\checkmark$	$\checkmark$	$\times$

## 3.2 Accuracy Investigation

As described in section 2.3.3, the relative uncertainty associated with the calculations can be obtained by using Equation 2.39. However, the estimate of the uncertainty is depending on how many calculations that are performed. The more calculations that are performed, the better estimation of the uncertainty. Therefore in the calibration software, there has to be a compromise between time and accuracy.

According to the LLN, both the number of iterations and the number of calculations per iteration should be large. However, it is not realistic to spend too long time to perform CF determination calculation for *in-situ* spectrometry measurements. Different combination of simulations and calculations per simulation was investigated for energies  $E = \{100, 779, 1048\}$  keV in order to get an idea about how the relative uncertainty in the uncertainty associated with the calculation of the CF varies with different combina-

tions.

The investigation was performed using the emergency preparedness model with inputs according to table 3.3. All parameter values were assumed to be uniformly distributed. For definition of the half-width of limit, see figure 3.4.

**Table 3.3:** Values used in the accuracy investigation. All parameter values were assumed to be uniformly distributed.

Parameter		Medium	Half-width of limits
Pressure	[kPa]	100	$\pm 5$
Temperature	[°C]	20	$\pm 10$
Relative humidity	[%]	80	0
Detector distance to the ground	[m]	1	$\pm 0.05$
Veg. height	[m]	0	–
Surface mass	[kg/m <sup>2</sup> ]	0	–
Activity content in veg.	[%]	0	–
Soil density	[kg/m <sup>3</sup> ]	900	$\pm 800$
Soil slab thickness	[m]	0.03	$\pm 0.02$
Activity content in soil	[%]	100	$\pm 0$

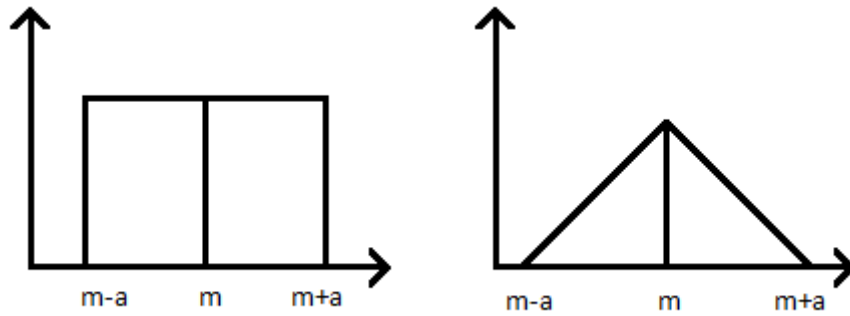


**Figure 3.4:** The probability density functions for uniform and triangular distribution.  $m$  is the expectation value or the medium and  $a$  is the half-width of limits.

### 3.2.1 Results and Discussions

Figure 3.5 shows the relative uncertainty of the combined uncertainty associated with the calibration factor. The number of calculations per simulation and the number of simulations were varied. It is possible to see in Figure 3.5 that the relative uncertainty

of the combined uncertainty is lower for large number of calculations and also larger number of calculations per simulation. Also, the relative uncertainties for simulations containing 100 and 120 calculations per simulation did not vary much. For increasing number of simulations, the relative uncertainty of the combined uncertainty should be decreasing, which means better estimation of the combined uncertainty. However, such trend could not be seen in Figure 3.5.

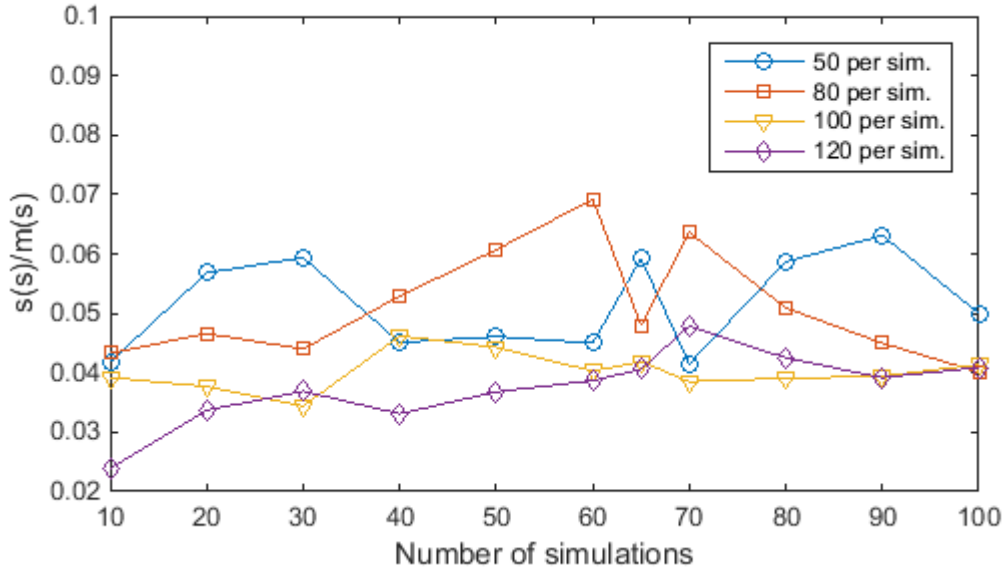


**Figure 3.5:** The relative uncertainty of the combined uncertainty associated with the calibration factor based on the preparedness model and the photon energy  $E = 100$  keV. The number of calculations per simulation and the number of simulations were varied.

Table 3.4 shows the calculation time and the standard deviation of the standard uncertainty associated with the calibration factor for some combinations of calculations. As can be seen in the Table 3.4, the standard deviation would not necessarily be reduced when the number of total calculations was increased, but the calculation time was increased much. Therefore, it is up to the user to decide about the the number of calculations per simulation and the number of simulations and thereby the accuracy of the estimation of the combined uncertainty associated with the calibration factor.

**Table 3.4:** Calculation results for photon energy  $E = 100$  keV.

Cal. $\times$ Sim.	Calculation time [s]	S. D.
100 $\times$ 50	275	0.0443
100 $\times$ 100	550	0.0414
120 $\times$ 50	330	0.0368
120 $\times$ 100	660	0.0409

## 4 | Results and Discussions

In this section, results from calibration factor calculation, detector field-of-view calculation and the combined uncertainties associated to calibration factor calculations are presented. Also a brief description of the developed graphical user interface is given.

### 4.1 Calibration Factor

Different calibration factors depending on the radioactivity deposition on/in the ground are shown in Figure 4.1, 4.2 and 4.3. In order to be able to compare different models, the same conditions were assumed for the models plotted in the same figure.

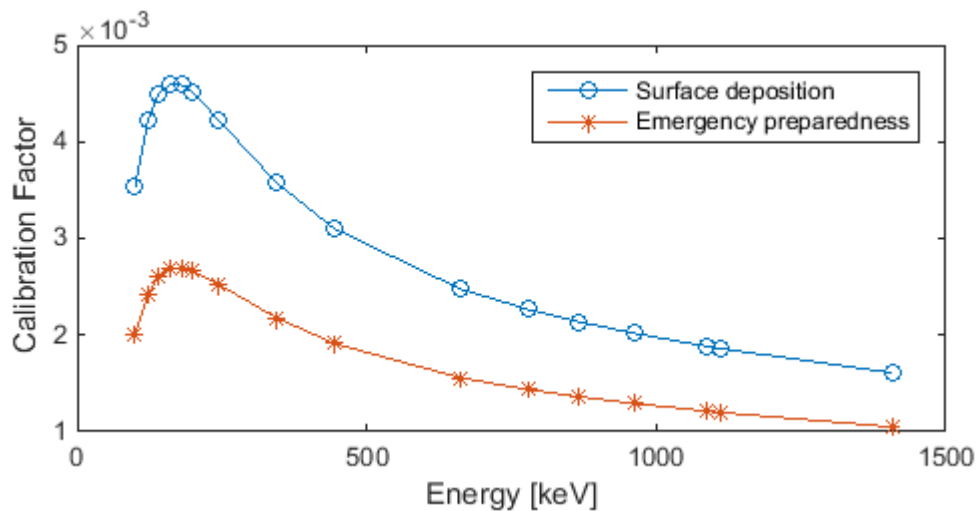


**Figure 4.1:** Calibration factors for surface deposition model and the emergency preparedness model plotted as function of photon incidence energy.

The calibration factors that were obtained using the surface deposition model and the emergency preparedness model can be seen in Figure 4.1. The results are similar to the ones that were obtained from a earlier study [6], though with small differences. These differences might depend on different description of the density of air that was used. As can be seen in Figure 4.1, the calibration factors calculated using surface deposition model are higher than those ones that were calculated with emergency preparedness

model. This is due to the fact that no attenuation in soil occurs in the surface deposition model.

In Figure 4.2 the calibration factors for exponential respective multiple slab model are shown for the case where the same detector might have been used. In order to obtain a description of how the radioactivity penetrates into the soil, empirical values [7] for activity contents were used. An exponential function was adapted to the empirical values so that the activity in the soil can be described in the form as in Equation 2.22. The data and the adaption of the data points is shown in Figure C.1, which can be found in Appendix C.

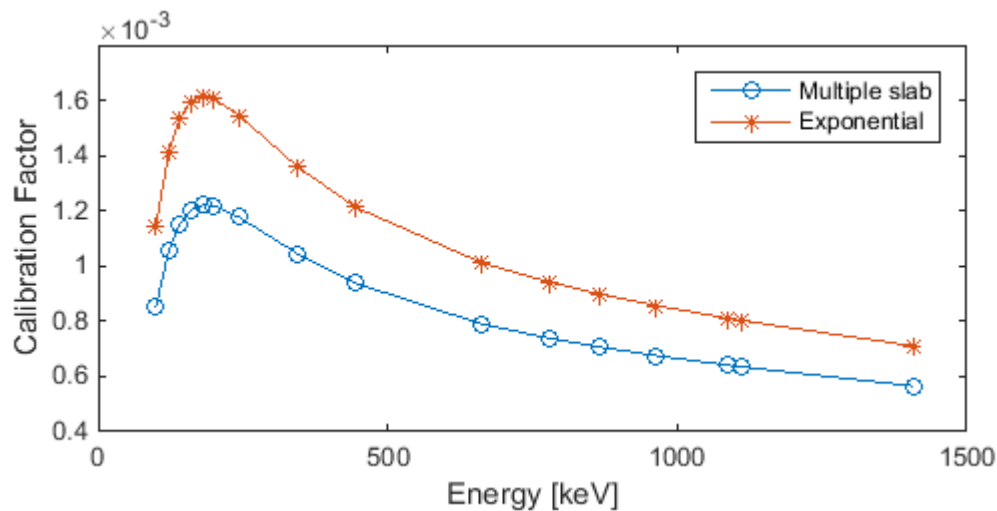


**Figure 4.2:** Calibration factors for multiple slabs model and the exponential model plotted as function of photon incidence energy. The relaxation length was adapted to empirical data from Boson *et al.* [7].

From Figure 4.2 one can see that the curves have similar shape, which is expected. For the same conditions, the exponential model gives higher calibration factors, about 30% more than calibration factors calculated using multiple slab model. It is because that there had been an overestimation of the activity near the ground surface in the data adaption. And in combination of low attenuation, the photon fluence rate for the exponential model might be overestimated and in turn the calibration factor. However, it is difficult to say how realistic the exponential model is due to the lack of empirical data of the calibration factors. The calibration factor calculated using the exponential model will vary depending on the exponential function that was adapted to the data points and also the soil density that was assumed. Since soil has a good attenuating ability, by assuming homogeneous soil density in depth will result an incorrect estimation of the photon fluence rate and thereby the calibration factor. This problem can be reduced by using relaxation mass depth instead of relaxation length [2].

The calibration factors for exponential model with several relaxation lengths are shown in Figure 4.3. Note that the surface deposition model can also be described as an exponential model with zero relaxation length. The calibration factors are decreasing with increasing relaxation lengths. The greater the relaxation length is, the deeper the radionuclides penetrate into the soil [5]. When the radionuclides penetrate deeper in the soil, it means that the possibility for them to be detected is lower because the attenuation of the soil. Therefore, the calibration factors are low for long relaxation lengths.

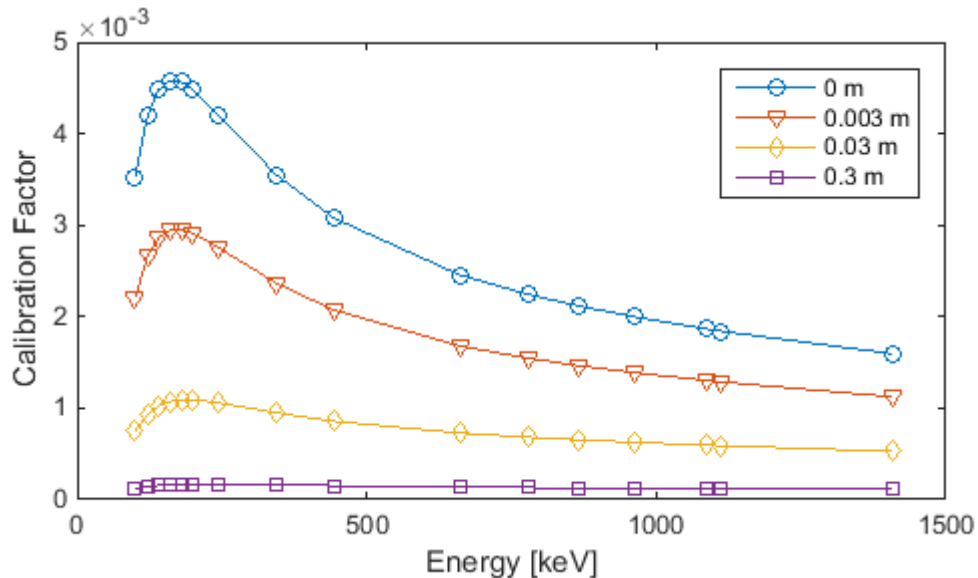


**Figure 4.3:** Calibration factors for the exponential model with varying radionuclide relaxation lengths plotted as function of photon incidence energy. The soil density was set to  $1500 \text{ kg/m}^3$  and the activity on the ground surface was constant.

#### 4.1.1 The Effects from Vegetation

Figure 4.4, 4.5 and 4.6 present the calibration factors calculated in the presence of radioactivity in the vegetation. The vegetation conditions were set to the same for all deposition models and the values are presented in Table 4.1.

**Table 4.1:** Values of vegetation condition used in the calculation of calibration factor in presence of vegetation.

Parameter	Value
Height [m]	0.1
Surface mass [ $\text{kg/m}^2$ ]	1
Activity content [%]	30

The calibration factors are always higher for calculation with radioactivity containing



vegetations than those without. This difference is barely visible for the surface deposition model, though. The attenuation coefficient for the vegetation under the conditions given in Table 4.1 is slightly higher than the coefficient for dry air. When the radioactivity is only deposited on the surface, the vegetation on the ground has small impact on the photon fluence rate that reaches the detector. The attenuation coefficient for the vegetation increases if the surface mass increases. However, the attenuation coefficient will be limited by the water content in the vegetation.

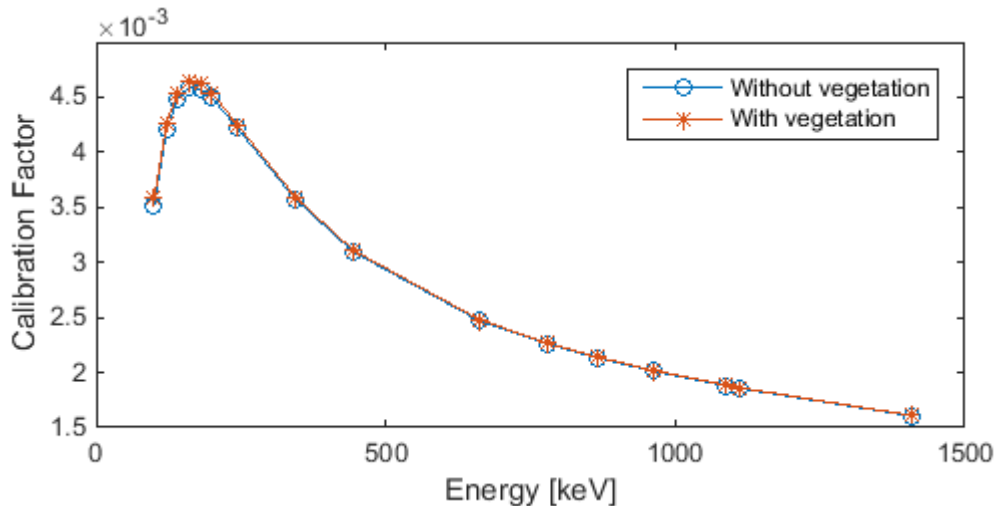


**Figure 4.4:** Comparison between calibration factors calculated with and without vegetation above the ground based on the surface deposition model.

Compared to the surface deposition model, the differences in calibration factors calculated with and without vegetation are more pronounced for the models which include radioactivity deposition in the ground. The reason for this is that the vegetation has much lower attenuation coefficient than the soil and that, in some extent, the activity accumulated in the vegetation has shorter distance to the detector. Both these factors give rise to increased photon fluence rate, and in turn increased calibration factor due to the proportionality between these two quantities.

For the multiple slabs model, the soil conditions were taken from an earlier study [7]. The difference is even larger compared to the surface and volume deposition model. The soil densities are much higher than the density assumed in the emergency preparedness model. And also the thickness of the layers are larger in the multiple slabs model which gives larger attenuation effects. These factors result in that the difference in calibration factors is even larger for the multiple slabs model, see Figure 4.6.

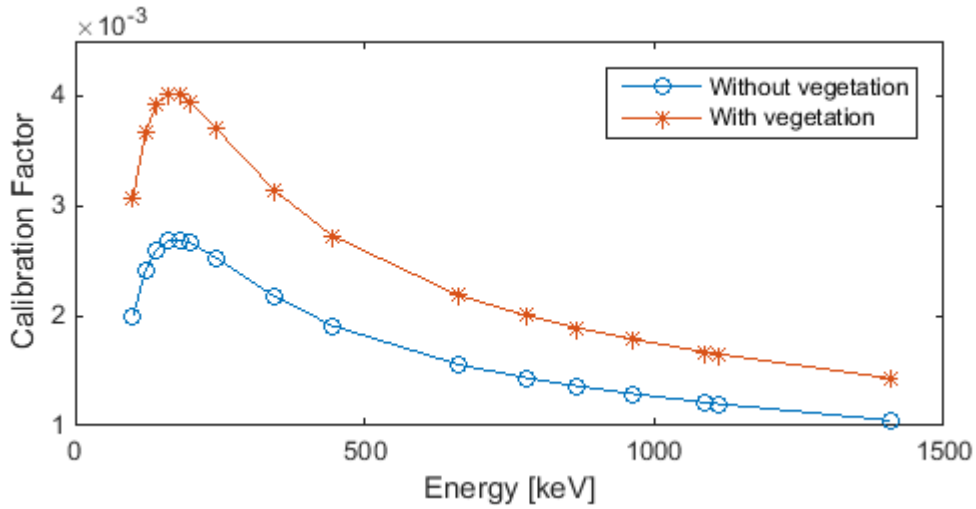


**Figure 4.5:** Comparison between calibration factors calculated with and without vegetation above the ground based on the emergency preparedness model.

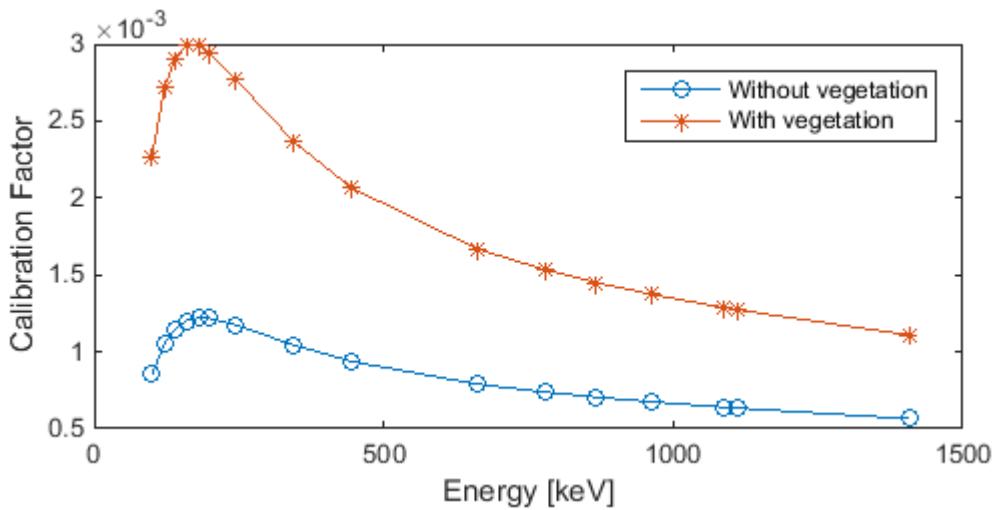


**Figure 4.6:** Comparison between calibration factors calculated with and without vegetation above the ground based on the multiple slabs model.

## 4.2 The Field-of-View of the Detector

Figure 4.7, 4.8 and 4.9 present the detector's field-of-view for several photon energies when assuming different deposition model. In these figures the contribution of full-energy peak count rate from remote region was plotted as a function of the field-of-view of the detector. The full-energy peak count rate contribution from remote region was defined as the ratio between the photons emitted from remote region that are registered by the

detector and the photons emitted from the whole plane. The field-of-view of the detector for some typical energies are tabulated in Appendix D.

It can be seen in Figure 4.7 and 4.8 that the photon contribution from remote region is decreasing more drastically for the emergency preparedness model. Also the field-of-view of the detector is larger for the surface deposition model for all photon energies. These effects depend on that the photon fluence rate is smaller for the emergency preparedness model where the attenuation in soil occurs. However, the surface deposition model is a simplified model, so the detector field-of-view is overestimated.

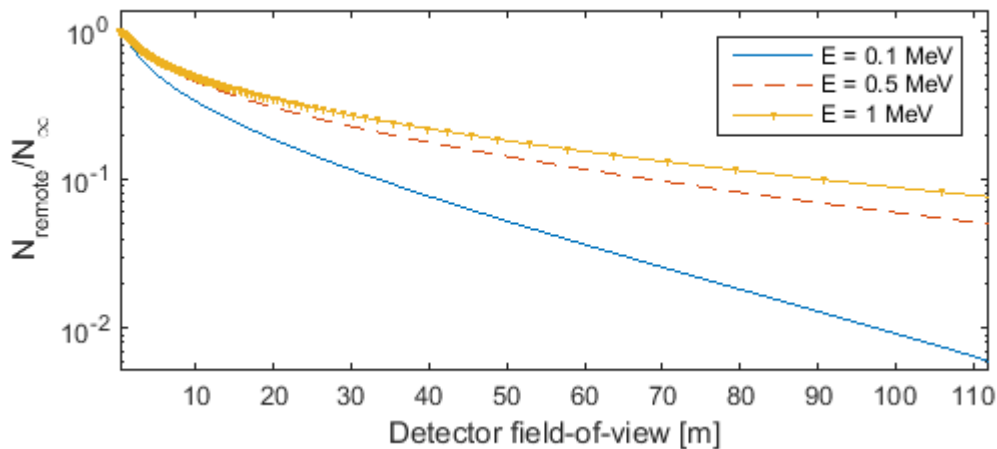


**Figure 4.7:** Full-energy peak count rate contribution from remote region as function of the detector field-of-view for three photon energies. Calculation based on the surface deposition model.

The field-of-view of the detector calculated based on exponential model are shown in Figure 4.9. Due to the fact that the radioactivity will diffuse and homogenise as time goes by, several relaxation lengths were tested in order to see how the photon contribution from remote regions varies with time. As can be seen in the figure, the field-of-view of the detector decreases as the relaxation length grows. The radionuclides penetrate deeper into the soil when the relaxation length is larger, which means that the photons emitted from deeper regions might be attenuated by the soil before the detector does response.

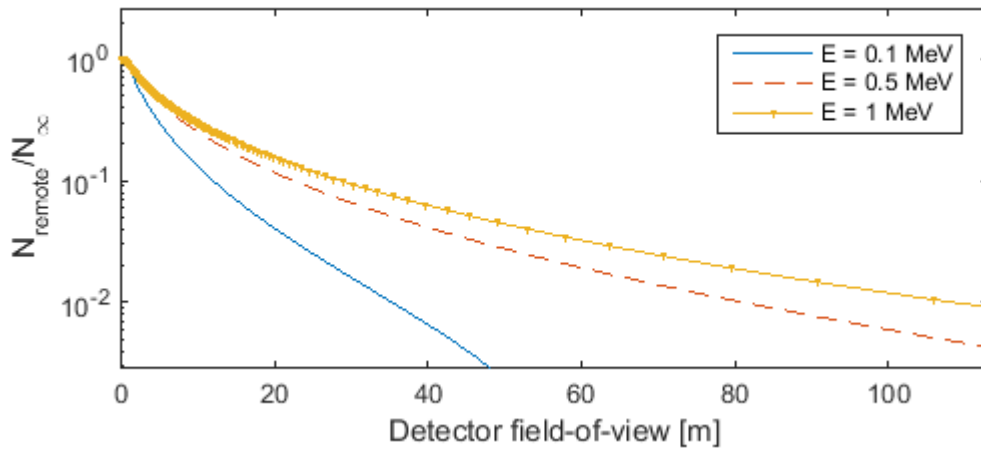


**Figure 4.8:** Full-energy peak count rate contribution from remote region as function of the detector field-of-view for three photon energies. Calculation based on the emergency preparedness model.

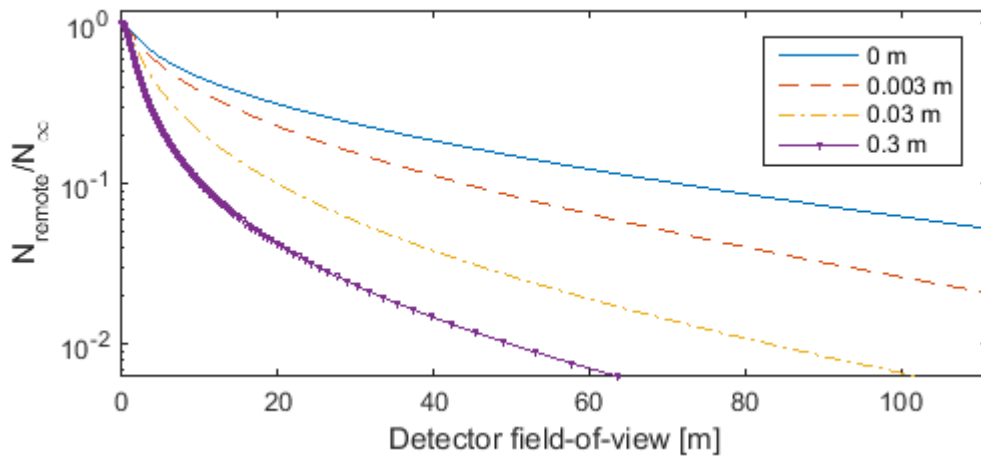


**Figure 4.9:** Full-energy peak count rate contribution from remote region as function of the detector field-of-view for photon energy  $E = 660$  keV. Calculation based on the exponential model with four different photon relaxation lengths.

### 4.3 Combined Uncertainties

The combined uncertainties are shown in Table E.1, E.2 and E.3, which can be found tables in Appendix E. In order to obtain the combined uncertainty associated to the calculation based on the surface deposition model and the emergency preparedness model, values in Table 4.2 were used. For calculation based on the multiple slabs model, values

for soil conditions were taking from an earlier study [7], while the other conditions were taking as shown in Table 4.2.

**Table 4.2:** Values used in the combined uncertainty investigation for the surface deposition model respective the emergency preparedness model. Parameters were assumed to be uniformly distributed.

Parameter		Medium	Limits
Pressure	[kPa]	100	$\pm 5$
Temperature	[°C]	7.5	$\pm 22.5$
Relative humidity	[%]	80	0
Detector height	[m]	1	$\pm 0.05$
Soil density	[kg/m <sup>3</sup> ]	900	$\pm 800$
Soil slab thickness	[m]	0.03	$\pm 0.02$
Activity content in soil	[%]	100	0

For the surface deposition model, the combined uncertainties for the whole calibration measurement were between 4.2% to 4.9% ( $k = 1$ ), depending of the photon energy and the number of calculations performed. Note that the uncertainty contribution from the detector efficiency determination was 4%. This means that the contribution of the uncertainty associated with the calibration factor calculation to the combined uncertainty is very small, because there are only uncertainties in the detector efficiency calibration, the air density and the distance between the detector and the source.

The combined uncertainties for calculations based on the emergency preparedness model have larger variations compare to the surface deposition model. They vary from 27% to 37% ( $k = 1$ ) depending on the photon energy and the total number of calculations. Because the difference between the two models is the soil attenuation, these "extra" uncertainties could only come from the uncertainty of the soil density. In order to cover the most types of soil, the uncertainty in the soil density was assumed to be large. This large uncertainty propagates further and results in a large combined uncertainty. The combined uncertainties are also in agreement with results from an earlier study [6].

As stated above, the uncertainty of the soil density has a large impact on the combined uncertainty, i.e. by lowering the uncertainty of the soil density the combined uncertainty will decrease. There is a lack of empirical data for the calibration factor assuming multiple slabs model using the HPGe detector that is considered in this project. But if one uses the detector characterised by Equation 2.3 and soil conditions taking from Boson *et al.* [7], the combined uncertainty for calculations based on the multiple slabs model will vary from 5.2% to 6.2% ( $k = 1$ ) depending on the photon energy and the total number of calculations. In the multiple slabs model, the soil column sample was divided in several sections. In this way, the uncertainty of the soil density in each

section can be lowered. Due to the lowered uncertainties, the combined uncertainty for the multiple slabs model is much lower compare to the emergency preparedness model even though there are more input quantities that are associated with uncertainties.

## 4.4 Graphical User Interface

User-friendly graphical user interfaces(GUIs) were designed for each deposition model. Figure 4.10 shows one of the GUIs. The GUIs have similar appearance and the execution options are the same for all of the models. Input quantities that can be sampled are shown in Table 3.2.

For every input photon energy, the program provides the calibration factor and the detector's field-of-view in external figures. The combined uncertainty is saved as a text file (*.txt*) for further use. More details about the program can be found in the User Manual in appendix F.

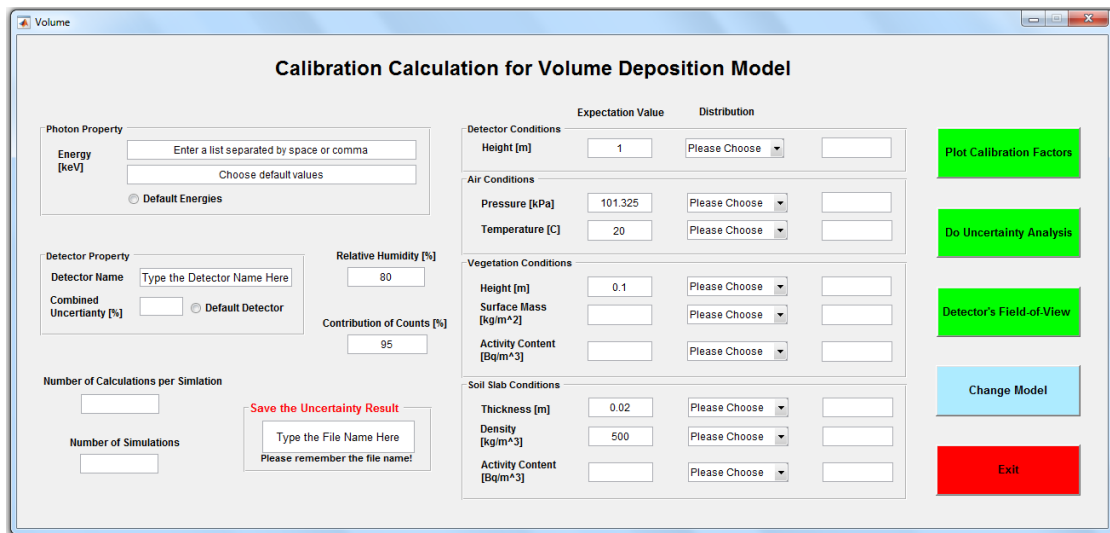


Figure 4.10: The GUI for the calculation for the volume deposition model.

## 5 | Conclusions

The designed software calculated the calibration factor well for the surface deposition model and the emergency preparedness model. Validation of the calibration factor must be performed for the multiple slabs model and the exponential model. The results of the effect of the vegetation and the field-of-view of the detector were reasonable, although validation need to be performed.

The combined measurement uncertainty based on the surface deposition model was calculated to be between 4.2% to 4.9% ( $k = 1$ ), depending on the photon energy. For the emergency preparedness model, the total measurement uncertainty was in the range 27% to 37% ( $k = 1$ ), depending on the photon energy. The high uncertainty in the soil density estimation contributed to a high combined measurement uncertainty when the calculation performed was based on the emergency preparedness model. This high uncertainty is due to the fact that the density assumed in the emergency preparedness model should cover many ground types. If the density is measured for soil samples, the uncertainty of the density will be reduced significantly resulting in a decreased combined measurement uncertainty for the emergency preparedness model. The combined uncertainty for the multiple slabs model and the exponential needs to be validated.

## 6 | Further Work

Due to the lack of empirical data during the time of this project, some quantities should be validated in the future. They are:

- the calibration factor and its combined uncertainty based on the multiple slabs model and the exponential model
- the calibration factor for models that include vegetations on the ground
- the field-of-view of the detector for all models

Also, some improvements should be done for a more user-friendly software, such as functions that can handle incorrect inputs.



# References

- [1] G. Choppin, J. O. Liljenzin, and J. Rydberg. *Radiochemistry and Nuclear Chemistry. Third Edition*. Butterworth-Heinemann.
- [2] ICRU. Gamma-ray spectrometry in the environment, icru report 53. Technical report, International Commission on Radiation Units and Measurements. 1994.
- [3] J. P. Laedermann, F. Byrde, and C. Murith. In-situ gamma-ray spectrometry: the influence of topography on the accuracy of activity determination. *Journal of Environmental Radioactivity*, 38(1):1–16, 1998.
- [4] J. H. Hubbell and S. M. Seltzer. X-ray attenuation and absorption for materials of dosimetric interest. Technical report, The National Institute of Standard and Technology (NIST). Available from <http://www.nist.gov/pml/data/xraycoef/>.
- [5] H. J. Beck, J. DeCampo, and C. Gogolak. In-situ Ge(Li) and NaI(Tl) gamma-ray spectrometry. HASL-258, Health and Safety Laboratory, US Atomic Energy Commission.
- [6] J. Boson, H. Ramebäck, T. Nylén, and K. Lidström. Kalibrering av en HPGe-detektor för gammaspektrometri i fält. FOI-R-2914-SE, FOI, Umeå, Sweden. 2010.
- [7] J. Boson, K. Lidström, T. Nylén, G. Ågren, and L. Johansson. In-situ gamma-ray spectrometry for environmental monitoring: A semi empirical calibration method. *Radiation Protection Dosimetry*.
- [8] W. Sowa, E. Martini, K. Gehreke, P. Marschner, and M. J. Naziry. Uncertainty of in situ gamma ray spectrometry for environmental monitoring. *Radiation Protection Dosimetry*, 27(2):93–101, 1989.
- [9] G. Sibbens and T. Altzitzoglou. Preparation of radioactive sources for radionuclide metrology. *Metrologia*, 44(1):71–79, 2007.
- [10] K. Lidström and T. Nylén. Beredskapsmetoder för mätning av radioaktivt nedfall. FOA-R-98-00956-861-SE, FOA, Umeå, Sweden. 1998.
- [11] Joint Committee for Guides in Metrology(JCGM). The guide to the expression of uncertainty in measurement(GUM). Available from [http://www.bipm.org/utis/common/documents/jcgm/JCGM\\_100\\_2008\\_E.pdf](http://www.bipm.org/utis/common/documents/jcgm/JCGM_100_2008_E.pdf).

- [12] Joint Committee for Guides in Metrology(JCGM). Evaluation of measurement data – supplement 1 to the ”guide to the expression of uncertainty in measurement” – propagation of distributions using a monte carlo method. Available from <http://www.bipm.org/en/publications/guides/gum.html>.
- [13] W. L. Dunn and J. K. Shultis. *Exploring Monte Carlo Method*. Elsevier.
- [14] K. Jareteg. Monte carlo simulations. Available from <http://klas.nephy.chalmers.se/teaching/montecarlo2013/documents/Slides.pdf>. Lecture Hand-out, 2013.
- [15] M. D. McKay, R. J. Beckman, and W. J. Conover. A comparison of three methods for selecting values of input variables in the analysis of output from a computer code. *Technometrics*.
- [16] Palisade. Latin Hypercube vs. Monte Carlo. Available from [http://www.palisade.com/downloads/help/risk35/faq\\_html/latinhypercubevs.montecarlo.htm](http://www.palisade.com/downloads/help/risk35/faq_html/latinhypercubevs.montecarlo.htm). [10 Oktober 2014].
- [17] J. A. Rice. *Mathematical Statistics and Data Analysis. Third Edition*. Thomson Higher Education.
- [18] Swedish Meteorological and Hydrological Institute. Lufttryck. Available from <http://www.smhi.se/kunskapsbanken/meteorologi/lufttryck-1.657>. [19 September 2014, written in Swedish].
- [19] Swedish Meteorological and Hydrological Institute. Luftfuktighet. Available from <http://www.smhi.se/kunskapsbanken/meteorologi/luftfuktighet-1.3910>. [19 September 2014, written in Swedish].

## Appendix A

**Table A.1:** Values for parameters in Eq.(2.3) [6]. Six significant figures are retained for further calculation. These parameters are valid for this particular detector, since different detectors will have different energy response as well as angular response.

Parameter	Value
$a_1$	33.9245
$a_2$	-0.0392096
$a_3$	0.0353600
$a_4$	0.00132088
$a_5$	-487.125
$a_6$	-0.0671579
$a_7$	8.10449
$a_8$	0.215457
$a_9$	6.83275
$a_{10}$	-11.5236
$a_{11}$	0.848338

**Table A.2:** Mass attenuation coefficients for water that were used to obtain the parameters in Eq.(2.14). The density of water was assumed to be  $1 \text{ g/cm}^3$ . [4]

Energy [MeV]	$\mu/\rho[\text{cm}^2/\text{g}]$
0.1	$1.707 \cdot 10^{-1}$
0.15	$1.505 \cdot 10^{-1}$
0.2	$1.370 \cdot 10^{-1}$
0.3	$1.186 \cdot 10^{-1}$
0.4	$1.061 \cdot 10^{-1}$
0.5	$9.687 \cdot 10^{-2}$
0.6	$8.956 \cdot 10^{-2}$
0.8	$7.865 \cdot 10^{-2}$
1.0	$7.072 \cdot 10^{-2}$
1.25	$6.323 \cdot 10^{-2}$
1.5	$5.754 \cdot 10^{-2}$
2.0	$4.942 \cdot 10^{-2}$
3.0	$3.969 \cdot 10^{-2}$

## Appendix B

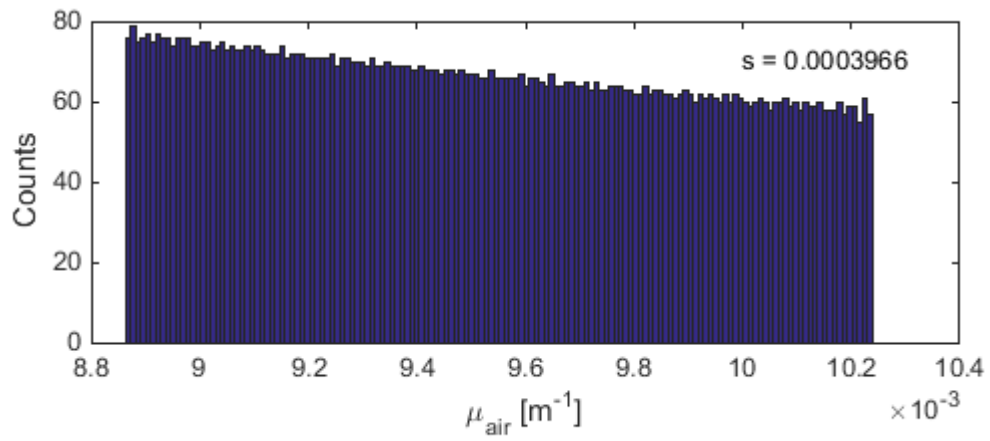


**Figure B.1:**  $\mu_{air}$  for photon energy  $E = 661$  keV calculated when the pressure was fixed. The standard deviation of the results is shown in the corner.

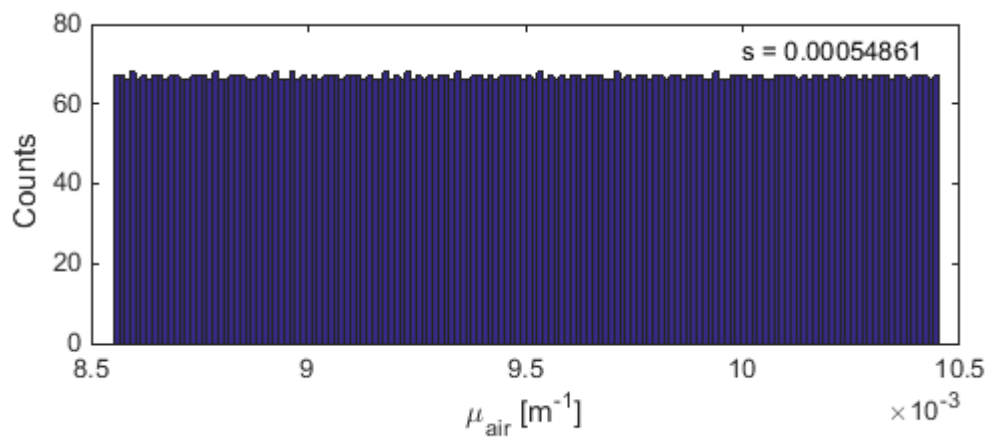


**Figure B.2:**  $\mu_{air}$  for photon energy  $E = 661$  keV calculated when the temperature was fixed. The standard deviation of the results is shown in the corner.

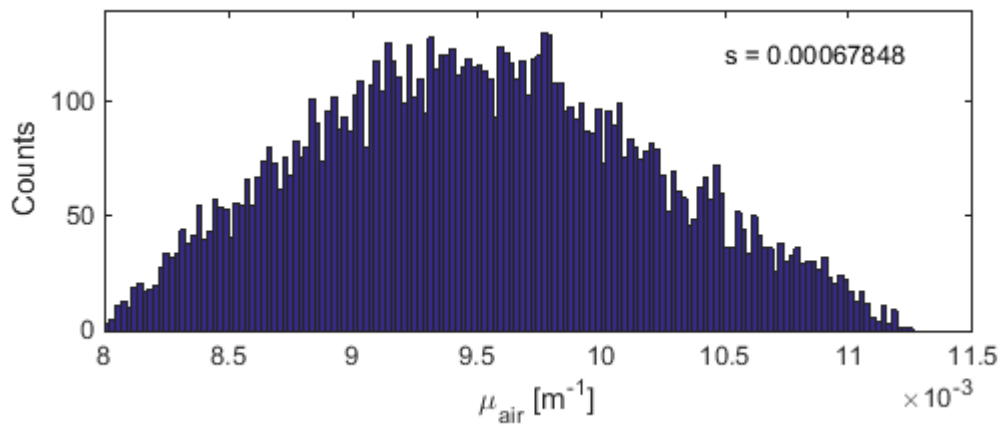


**Figure B.3:**  $\mu_{air}$  for photon energy  $E = 661$  keV calculated when the pressure was fixed. The standard deviation of the results is shown in the corner.

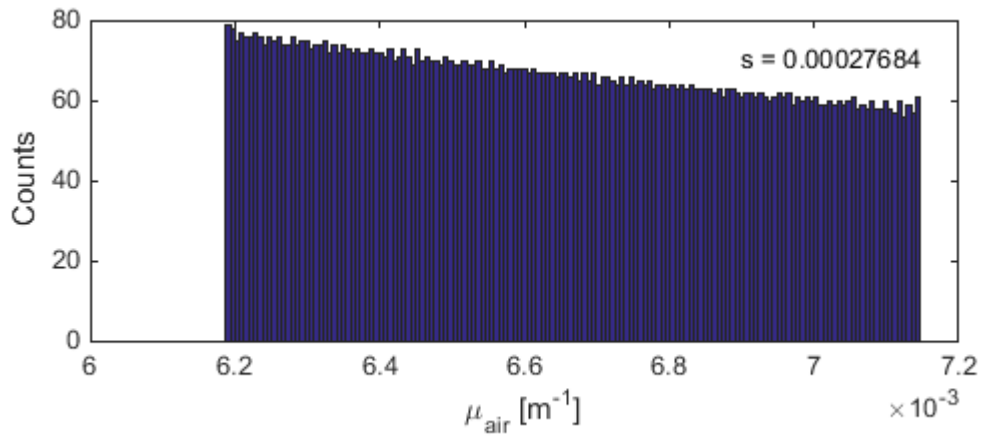


**Figure B.4:**  $\mu_{air}$  for photon energy  $E = 1048$  keV calculated when the relative humidity was fixed. The standard deviation of the results is shown in the corner.

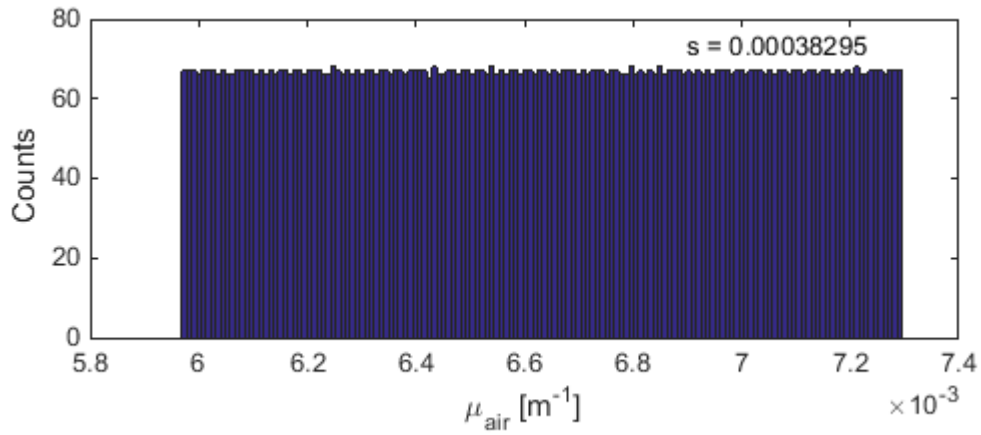


**Figure B.5:**  $\mu_{air}$  for photon energy  $E = 1048$  keV calculated when the temperature was fixed. The standard deviation of the results is shown in the corner.

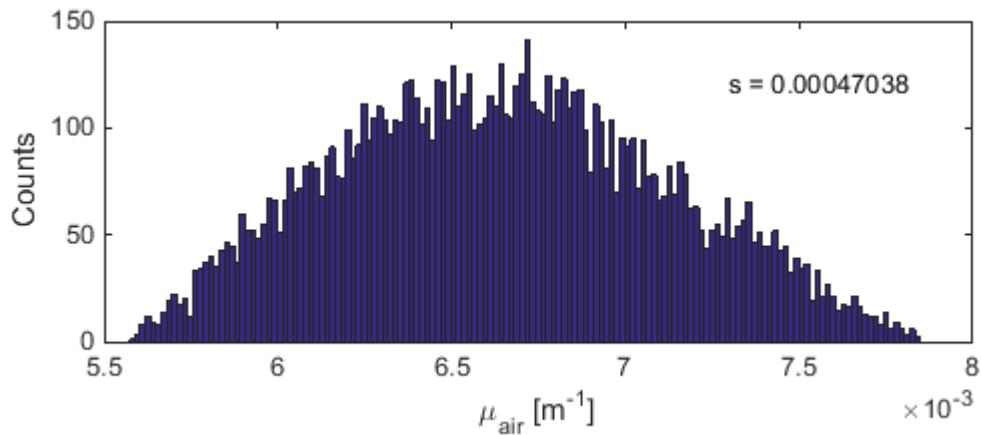


**Figure B.6:**  $\mu_{air}$  for photon energy  $E = 1048$  keV calculated when the relative humidity was fixed. The standard deviation of the results is shown in the corner.

## Appendix C

**Table C.1:** Values from Boson *et al.*, [7] that were used to obtain the input data for the exponential model.

Slab	Thickness [cm]	Density [kg/m <sup>3</sup> ]	Fraction of total activity [%]
1	2.0	1210	80
2	5.0	1460	16
3	9.4	1720	4

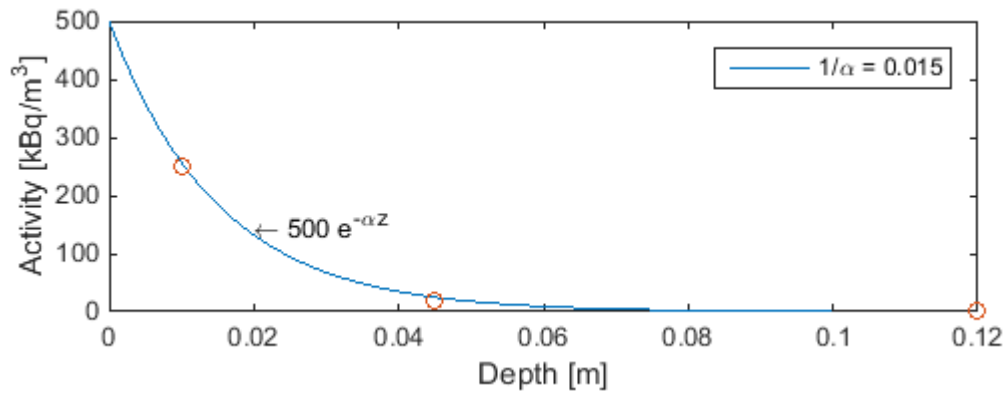


**Figure C.1:** Adaption of an exponential function to data points from Boson *et al.* [7].

**Table C.2:** Input values that were used in the exponential model for comparison between the multiple slabs model and the exponential model.

Density [kg/m <sup>3</sup> ]	1500
A <sub>0</sub> [Bq/m <sup>3</sup> ]	500
Relaxation length [m]	0.015



## Appendix D

**Table D.1:** The field-of-view of the detector corresponding to 95% contribution of full-energy peaks for all models. Soil conditions for multi-slab model were taken from an earlier study [7]. Relaxation length was taken as 0.3 cm and the soil density  $1500 \text{ kg/m}^3$  for the exponential model. Beside these, all other conditions were taken the same for all models.

Energy [keV]	Detector Field-of-View [m]			
	Surface dep.	Preparedness	Multi-slabs	Exponential
100	50.56	17.82	-	14.00
122	56.14	19.59	12.88	15.29
140	60.32	20.88	13.68	16.24
160	64.63	22.17	14.49	17.19
180	78.62	23.36	15.22	18.05
200	72.34	24.46	15.89	18.84
244	79.74	26.61	17.13	20.39
344	93.70	30.63	19.52	23.20
444	105.10	33.87	21.34	25.41
661	124.91	39.43	24.32	29.09
779	134.00	41.93	25.62	30.70
867	140.06	43.62	26.49	31.79
964	146.38	45.37	27.37	32.90
1086	153.76	47.40	28.38	34.18
1112	155.27	47.82	28.58	34.44
1408	170.90	52.14	30.70	37.12

## Appendix E

**Table E.1:** The combined uncertainty ( $k = 1$ ) for the calibration factor calculation for some typical photon energies, based on total 500 calculations.

Energy [keV]	Combined Uncertainty [%]		
	Surface dep.	Preparedness	Multi-slabs
122	4.46	37.45	6.23
344	4.14	32.16	5.68
661	4.28	29.29	5.41
779	4.27	28.62	5.35
964	4.27	27.78	5.28
1112	4.26	27.73	5.23

**Table E.2:** The combined uncertainty ( $k = 1$ ) for the calibration factor calculation for some typical photon energies, based on total 1000 calculations.

Energy [keV]	Combined Uncertainty [%]		
	Surface dep.	Preparedness	Multi-slabs
122	4.47	37.09	6.20
344	4.37	31.80	5.66
661	4.30	28.95	5.39
779	4.30	28.28	5.33
964	4.26	27.44	5.26
1112	4.25	26.90	5.21

**Table E.3:** The combined uncertainty ( $k = 1$ ) for the calibration factor calculation for some typical photon energies, based on total 2000 calculations.

Energy [keV]	Combined Uncertainty [%]		
	Surface dep.	Preparedness	Multi-slabs
122	4.45	36.64	6.17
344	4.34	31.40	5.64
661	4.28	28.58	5.38
779	4.27	27.92	5.32
964	4.25	27.09	5.24
1112	4.24	26.55	5.20

## Appendix X

# User Manual

Software for Calibration  
in *In-situ* Gamma-Ray Spectrometry

This manual is aimed to give guidance for using the software for calibration of gamma-ray spectrometric *in-situ* measurements. MatLab, version R2012b or later, is required to run this software since it was designed and comprises MatLab GUI.

The software is designed to be able to handle photons with energy up to 3 MeV, in other words, it can be used for most relevant photon energies in environmental measurements. However, one limitation is the energy range for which the intrinsic calibration of the HPGe detector was done for. For each input energy, the software has three outputs: the detector field-of-view, the calibration factor and the combined standard uncertainty for these measurands. The calibration factor is the total measurement efficiency which is an important parameter when comes to activity determination on site.

For calculation of the combined standard uncertainties, the method Latin Hypercube sampling is used. Parameters that contribute to the combined standard uncertainty can be sampled from three continuous probability distributions. The results are then saved in an external text file for further use.

## Getting Started

Find the file *main.m* and open it in MatLab by a double click. Click on the icon *run* to run the script/software. However, depending on the MatLab version, this icon will have different appearance.

After you had started the software, a menu window appears. See Figure F.1 for how the *run* button and the menu window appears in the MatLab version R2014b.

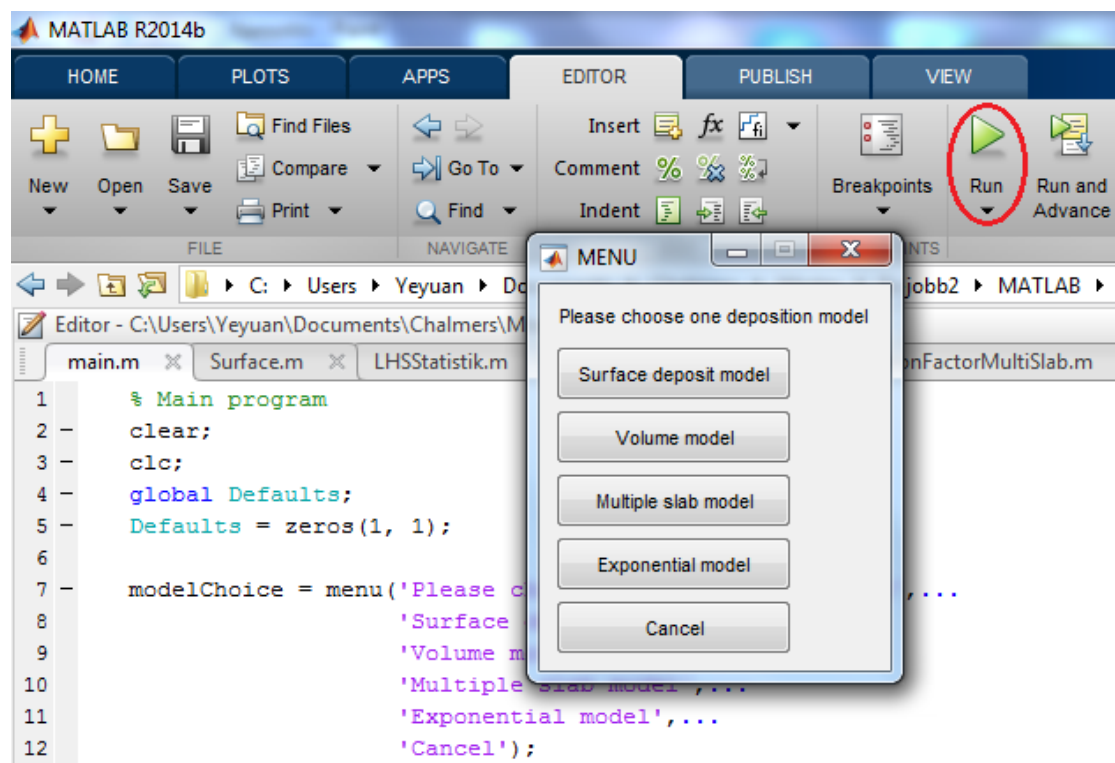


Figure F.1: The *run* icon and the main menu.

### Menu

There are five option buttons in the menu window, four deposition model buttons and one cancel button.

- Models** Choose the desired model by clicking the corresponding button, then a graphical user interface where you do the inputs for the chosen deposition model is opened.
- Cancel** You will receive a request, if answer "Yes", the software shuts down.

## Graphical User Interface

One of the Graphical user interfaces (GUI) is shown in figure F.2. The interfaces have different layout depending on the selected deposition model, but the differences are small.

The input boxes are arranged in panels in order to give you a better input overview. There are already default values in some of the boxes, the calculations will be performed using these values if you do not change them.

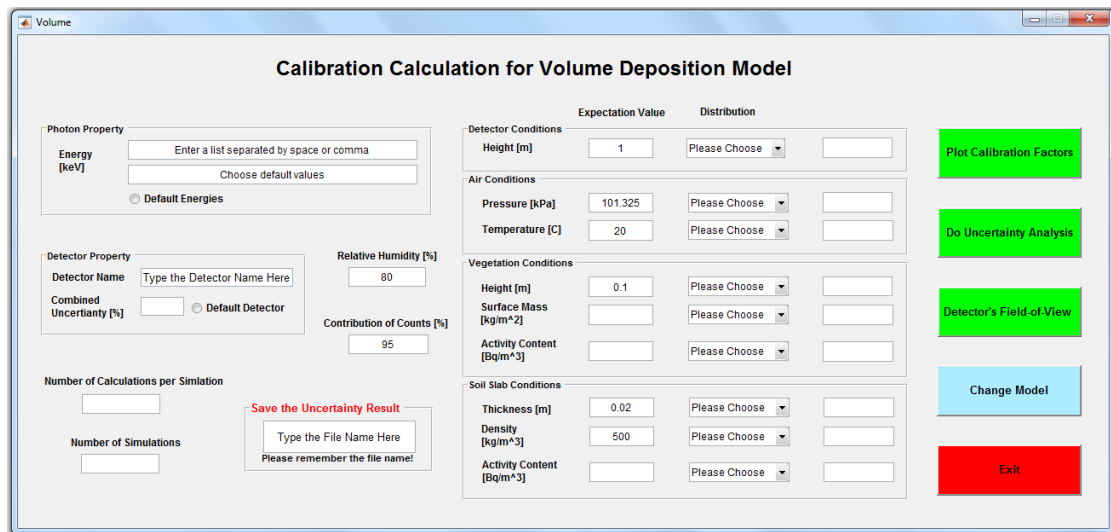


Figure F.2: User interface for a volume deposition model.

There are always five execution options, see the colored push buttons in figure F.2. Their functions are described briefly below.

- |                                 |  |
|---------------------------------|--|
| <b>Plot Calibration Factors</b> | An external window with plot of calibration factor versus photon energy is opened.                       |
| <b>Do Uncertainty Analysis</b>  | Simulate the combined standard uncertainty for each input energy.  |
| <b>Detector Field-of-View</b>   | An external window with a table showing the detector field-of-view for corresponding energies is opened. |
| <b>Change Model</b>             | Back to the main menu for model change.  |
| <b>Exit</b>                     | Exit the GUI and the software shuts down.  |

## How to Enter Input Data

Follow the advice below in order to avoid any unsuccessful calculations. Figure F.3 show the left part of a GUI.

The image shows a GUI interface with several sections:

- Photon Property**:
  - Energy [keV]**: A text input field with the placeholder text "Enter a list separated by space or comma".
  - A second text input field with the placeholder text "Choose default values".
  - A radio button labeled "Default Energies".
- Detector Property**:
  - Detector Name**: A text input field with the placeholder text "Type the Detector Name Here".
  - Combined Uncertainty [%]**: A text input field.
  - A radio button labeled "Default Detector".
- Relative Humidity [%]**: A text input field containing the value "80".
- Contribution of Counts [%]**: A text input field containing the value "95".
- Number of Calculations per Simulation**: A text input field.
- Number of Simulations**: A text input field.
- Save the Uncertainty Result**: A text input field with the placeholder text "Type the File Name Here" and a note below it: "Please remember the file name!".

Figure F.3: The left part of a GUI.

### Input for the photon property

- Energy** Input desired photon energies as a list separated by space or comma in the unit [keV].
- Defaults** Choose the preprogrammed photon energies by pressing the radio buttons. The default energies are: {100 122 140 160 180 200 244 344 444 661 779 867 964 1086 1112 1408} [keV]. These energies will be displayed in the boxes under the input boxes for energy. Please do not change any number in this box.



## Input for the detector name

Due to the fact that all detectors are unique, the detector efficiency will depend on the detector characteristic. Default detector in this case is a HPGe detector made by Ortec Inc., USA.

<b>Detector Name</b>	Input the name of the detector.
<b>Default Detector</b>	The HPGe detector named defaultDetector, which was produced by Ortec Inc., USA.

redJa, man kan lägga till nya detectorer, sedan är det bara att anropa den i programmet. You can add another detector by writing a MatLab function file for the detector efficiency calculation. Give the function the same name as the detector. There must be two input argument to the detector efficiency function, set the photon incidence angle with unit radian as the first input argument to the function, and set the photon energy with unit MeV as the second input argument. There is an example below.

### **Example:**

```
function y = defaultDetector(theta, e)
% defaultDetector determines the intrinsic efficiency detector for
% the default detector from empirical studies
% defaultDetector(Theta, E) returns the detector efficiency
% with photon incidence angle, Theta, in [rad] and the photon
% energy, E, in [MeV]

% A = parameters
A = [33.9245, -0.0392096, 0.0353600, -0.00132088, -487.125, ...
     -0.0671579, 8.10449, 0.215457, 6.83275, -11.5236, 0.848338];

E = e*1000; % convert to [keV]

y = exp(A(1) + A(2)*theta.^2 + A(3).*theta + A(4).*E + ...
        A(5)./E + A(6)*cos(A(7)*theta./E.^A(8) - A(9)) + ...
        A(10)*log(E) + A(11)*(log(E)).^2);
end
```

## Input for the name of the uncertainty result

Regarding the uncertainty analysis the result will be saved as a text file, and the desired file name will be given in this panel. You can use any symbol when you do your input, but please do remember the name of the file.

**File Name** Input desired name for the file in where the uncertainty analysis result is saved. If the name already exists, the content of the old one will be overwritten.

## Other inputs

**Number of Calculations per Simulation** Enter the desired number of calculations per simulation. The probability density functions of every input quantities are divided into the number that is entered here.

**Number of Simulation** Enter the desired number of simulations.

**Contribution of Counts** Enter the desired field-of-view in percent. The detector field-of-view is defined as the radius of a circle where the contribution of counts from its area is a certain percentage of the number of the counts from a circle with infinite radius.

**Relative Humidity** Enter the relative humidity for the air density calculation. Default value 80% can be used since this parameter does not have a significant effect on the result.

The middle part of the interface is constructed as a table with three columns. A general rule is to first input the expectation value, or the nominal value, of the parameter. Thereafter you choose the distribution in the pop-up menus. The parameters can have uniform, triangular and normal distributions. Depending the selected distribution, you are asked to enter either the half-width of limits or standard uncertainties of the distribution in the third column. For the meaning of half-width of limits, please see figure F.4.

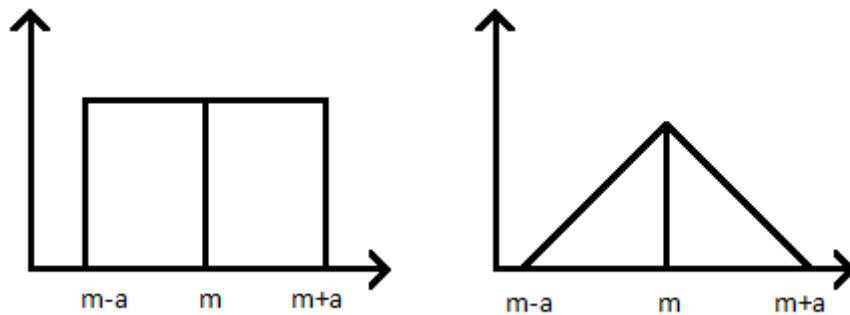


**Figure F.4:** The probability density functions for uniform and triangular distribution.  $m$  is the expectation value or the medium and  $a$  is the half-width of limits.

### Input for the detector distance to the ground

**Detector Height** Enter detector distance to the ground in meters. Choose the probability distribution and fill in the half-width limits or standard uncertainty. Default value for the detector distance to the ground is 1 m.

	Expected Value	Distribution	
<b>Detector Conditions</b>			
Height [m]	<input type="text" value="1"/>	Please Choose ▾	<input type="text"/>
<b>Air Conditions</b>			
Pressure [kPa]	<input type="text" value="101.325"/>	Please Choose ▾	<input type="text"/>
Temperature [C]	<input type="text" value="20"/>	Please Choose ▾	<input type="text"/>

**Figure F.5:** The panel for detector and air condition inputs.

### Input for the air conditions

- Pressure** Input the air pressure in kPa. Choose the probability distribution and fill in the half-width limits or standard uncertainty. Default value for the air pressure is 101.325 kPa.
- Temperature** Input the air temperature in °C. Choose the probability distribution and fill in the half-width limits or standard uncertainty. Default value for the air temperature is 20°C.

### Input for the vegetation conditions

Due to the algebraic limitations, the vegetation height must be non-zero. If there is not any vegetation, set the surface mass to zero instead. The activity content in the vegetation slab will then be set to zero automatically, as well as their ranges or variances.

	Expected Value	Distribution	
<b>Vegetation Conditions</b>			
<b>Height [m]</b>	<input type="text" value="0.1"/>	<input type="text" value="Please Choose"/> ▼	<input type="text"/>
<b>Surface Mass [kg/m<sup>2</sup>]</b>	<input type="text"/>	<input type="text" value="Please Choose"/> ▼	<input type="text"/>
<b>Activity Content [Bq/m<sup>3</sup>]</b>	<input type="text"/>	<input type="text" value="Please Choose"/> ▼	<input type="text"/>

**Figure F.6:** An example of the panel for vegetation condition inputs.

<b>Height</b>	Input the vegetation height in meters. Choose the probability distribution and fill in the half-width limits or standard uncertainty. Default value for the vegetation height is 0.1 m.
<b>Surface Mass</b>	Input the surface mass in $\text{kg}/\text{m}^2$ . Choose the probability distribution and fill in the half-width limits or standard uncertainty. Set surface mass to $0 \text{ kg}/\text{m}^3$ if there is not any vegetation on the ground.
<b>Activity Content</b>	Input the activity content in $\text{Bq}/\text{m}^3$ or proportion in the vegetation slab. Choose the probability distribution and fill in the half-width limits or standard uncertainty. Set activity content to 0% if there is not any activity content in the vegetation on the ground.

### Input for the soil conditions

The panels where you enter soil condition inputs have different appearance depending on the selected deposition model. The default values will also be different. For the surface deposition model, the soil slab thickness is infinite small and the soil density is  $1000 \text{ kg}/\text{m}^3$ . For the volume deposition model, the soil slab thickness is 0.02 m and the soil density is  $500 \text{ kg}/\text{m}^3$  which are the values for calculation using emergency preparedness model.

For multiple slab model the soil condition must be specified for every slab. Enter the values as a list separated by space or comma. When you fill in the number of slabs the software will remind you how to enter the soil conditions.

	Expected Value	Distribution	
<b>Soil Slab Conditions</b>			
<b>Thickness [m]</b>	<input type="text" value="0.02"/>	<input type="text" value="Please Choose"/> ▼	<input type="text"/>
<b>Density [kg/m<sup>3</sup>]</b>	<input type="text" value="500"/>	<input type="text" value="Please Choose"/> ▼	<input type="text"/>
<b>Activity Content [Bq/m<sup>3</sup>]</b>	<input type="text"/>	<input type="text" value="Please Choose"/> ▼	<input type="text"/>

**Figure F.7:** The panel for soil condition inputs for the volume deposition model.

- Thickness** Enter the soil slab thickness in m. Choose the probability distribution and fill in the half-width limits or standard uncertainty.
- Density** Enter the density in  $\text{kg/m}^3$ . Choose the probability distribution and fill in the half-width limits or standard uncertainty.
- Activity Content** Enter the activity content in  $\text{Bq/m}^3$  or relative activity content in the soil slab (or slabs). Choose the probability distribution and fill in the half-width limits or standard uncertainty.

### Input for the exponential model

In this case, activities penetrate exponentially into the soil. The vegetation contains no activity. The soil density is assumed to be uniformly distributed.

- Relaxation Length** Enter the relaxation length in cm. Choose the probability distribution and fill in the half-width limits or standard uncertainty.

## Calculations

For parameters that consist of uncertainties, the expectation (nominal) values are used for calculation of the calibration factor and the detector field-of-view. This means that both the calibration factor and the detector field-of-view are also expectation values.

For calculation of the combined uncertainty associated to the calibration factor determination, the square root of the total number of calculations was taken and round to the closest integer. This integer will be the number of iterations as well as the number of calculations per iteration. Because the uncertainty calculation time is long, the progress is shown in an external window during calculations. When the calculation is completed, the user will be reminded regarding the file name with the results.

## Outputs

Two kinds of outputs are given: A figure with calibration factors and a table with detector field-of-view, see figure F.8. These figures are not saved automatically. In order to save them, click *Save As...* under *File* in the menu in the figure window, see figure F.9. Note that the default file type is *.fig*, which must be opened in MatLab. Therefore if you want to open the figure in a common photo viewer it is convenient to choose other file type that is more general, such as *.jpg* or *.png*.

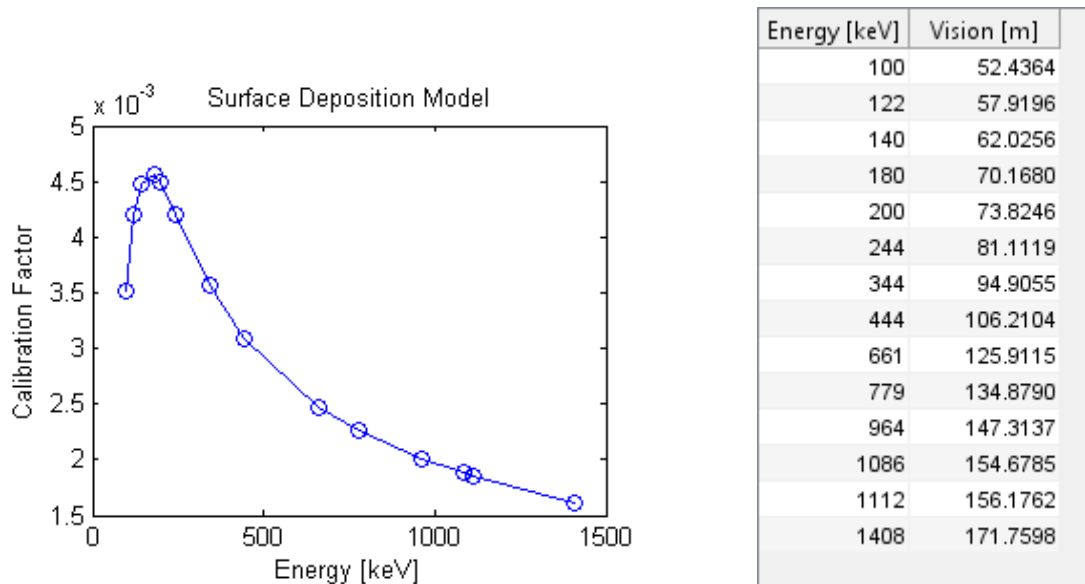


**Figure F.8:** Examples of the outputs, one plot and one table.

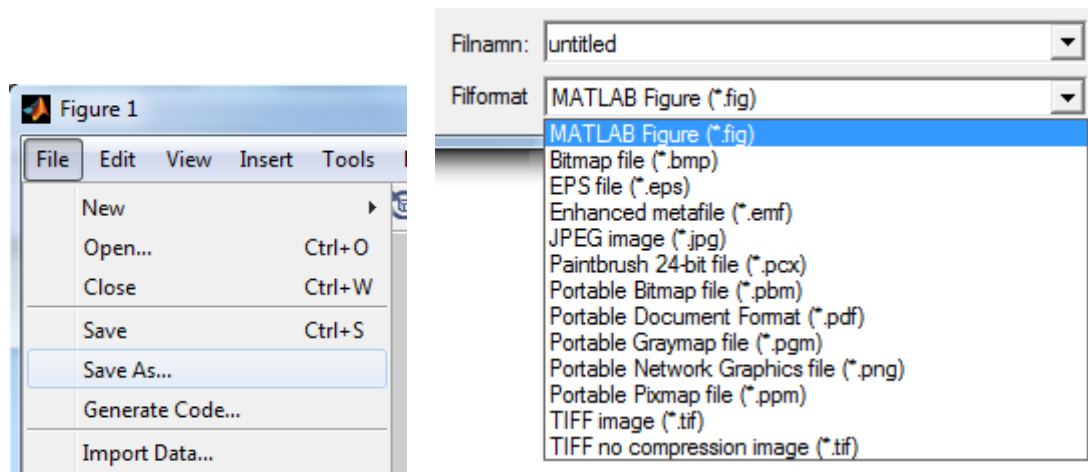


Figure F.9: LALA

The results of the combined uncertainty associated to the calibration factor calculation are saved in the sub-folders with the same name as the deposition model that was chosen. These sub-folders can be found in the folder named **Results**. There are three columns in the text file: photon energy given in keV, the nominal calibration factor and the combined uncertainties ( $k = 1$ ) given in %. An example is shown below.

100.00	3.482E-03	4.476
122.00	4.160E-03	4.458
140.00	4.430E-03	4.444
160.00	4.539E-03	4.430
180.00	4.528E-03	4.418